

Granite-Related Tin Metallogenic Events and Key Controlling Factors in Peninsular Malaysia, Southeast Asia: New Insights from Cassiterite U-Pb Dating and Zircon Geochemistry

Jie-Hua Yang^{a,b,*}, Mei-Fu Zhou^b, Rui-Zhong Hu^a, Hong Zhong^a, Anthony E. Williams-Jones^c, Liang Liu^a, Xing-Chun Zhang^a, Ya-Zhou Fu^a, Wei Mao^a

^a State Key Laboratory of Ore Deposit Geochemistry, Institute of Geochemistry, Chinese Academy of Sciences. Guiyang 550081, China

^b Department of Earth Sciences, The University of Hong Kong, Hong Kong, China

^c Earth and Planetary Sciences, McGill University, Montréal, Québec, Canada

***Corresponding author:** yangjiehua@vip.gyig.ac.cn (J.-H. Yang)

Abstract:

Permian-Triassic granites and associated tin deposits are widespread in the eastern Tethyan domain of Peninsular Malaysia. The ages of tin mineralization, however, are poorly constrained. Here we present the first precise cassiterite and zircon U-Pb ages for this mineralization, together with zircon Hf isotope and trace element data, which we use to constrain the timing and controls on tin mineralization in the context of the Paleo-Tethyan evolution. Cassiterite separates from the Sintok, Rahman, Bandi, Setahum, Lembing and Cherul tin deposits yielded U-Pb ages of 281.9 ± 3.4 Ma, 226.8 ± 7.6 Ma, 213.1 ± 3.9 Ma, 270.6 ± 4.6 Ma, 282.7 ± 4.6 Ma and 281.3 ± 8.5 Ma, respectively. These ages suggest that tin mineralization in Peninsular Malaysia occurred mainly occur between 230 and 210 Ma and between 290 and 270 Ma. Zircon

crystals from tin-bearing granites in the Cherul and Sintok plutons yielded U-Pb ages of 270 ± 1.0 Ma and 221.9 ± 0.6 Ma, respectively, which are consistent with the cassiterite U-Pb ages within the reported uncertainty. Zircon crystals from barren granites yielded a U-Pb age of 260.5 ± 0.7 Ma, which is between two tin mineralization periods. The barren granites have $\epsilon_{\text{Hf}}(t)$ values from -5.4 to +3.6, T_{DM2} values from 1.4 to 1.0 Ga and $\text{Ce}^{4+}/\text{Ce}^{3+}$ ratios from 40 to 120. By comparison, zircon crystals from the tin-bearing granites have low $\epsilon_{\text{Hf}}(t)$ values (-9.7 to -3.2) and $\text{Ce}^{4+}/\text{Ce}^{3+}$ ratios (4 to 67) and two-stage Hf model ages (T_{DM2}) of 1.4 to 1.8 Ga. We propose that the tin-bearing granites were derived from reduced magmas formed by the reworking of a sedimentary rock-dominated ancient crust. Thus, the factors controlling the formation of the tin-rich granites and the related tin deposits were the magma source and the redox state. The two periods of tin mineralization and associated magmatism in Peninsular Malaysia resulted from crustal anatexis in response to Paleo-Tethyan subduction and post-collisional crustal extension.

Keywords: Cassiterite U-Pb age, Controlling factors, Tin mineralization, Malaysia, SE Asia

1. Introduction

The Southeast Asian tin belt in the eastern Tethyan domain, extending from Myanmar and Thailand through Peninsular Malaysia to the Indonesian Tin Islands, is the world's largest producer of tin, in terms of both production and reserves.

According to the United States Geological Survey, 43% of world tin production in 2018 was sourced from this region, and SE Asia hosts 28% of the world's total tin reserves (Reference).

Previous studies have significantly advanced our understanding of tin mineralization in SE Asia (Hosking, 1973; Rajah et al., 1977; Schwartz and Askury, 1990; Lehmann et al., 1994; Linnen and Williams-Jones, 1995; Schwartz et al., 1995). However, the timing of tin mineralization in this belt has not been dated directly and is only inferred from the zircon U-Pb ages of granites. The precise age(s) of the tin mineralization, therefore, remains unknown, and consequently its genetic relationship to the Tethyan evolution is unclear.

The vast majority of tin deposits in SE Asia are thought to be temporally and compositionally related to B, Li, F, Cs and Sn-rich granitic rocks (Schwartz et al., 1995; Ng et al., 2017). In view of this, it has been proposed that the tin is of magmatic origin (Taylor, 1979; Hutchison, 1988b) and that magma evolution exerts a fundamental control in determining whether a granite is tin-fertile (Lehmann and Harmanto, 1990; Lehmann et al., 1994). The factors controlling the tin-fertility of the granites, however, are still understood, and need to be identified to provide a better understanding of tin-bearing granite metallogeny.

In this study, cassiterite U-Pb isotopic analyses were used to determine the ages of tin mineralization in Peninsular Malaysia directly. These ages were used in conjunction with zircon U-Pb ages of tin-bearing and barren granites in Peninsular Malaysia to establish the temporal relationships of the granites to the tin

mineralization. Building on this information, the Hf isotope and trace element compositions of the two classes of granite (tin-bearing and barren) were used to determine the key factors controlling the tin metallogeny and its relationship to the Paleo-Tethyan evolution.

2. Geological background

2.1 Regional geology

Southeast Asia is composed of several Precambrian continental blocks that were separated from the Gondwana supercontinent as result of three successive ocean basin opened and subsequent oceanic crust consumption [Paleo-Tethys (Devonian-Triassic), Meso-Tethys (late Early Permian- Late Cretaceous) and Neo-Tethys (Late Triassic – Late Cretaceous)] (Metcalf, 2013a). The main continental blocks that form the continental core of SE Asia (Sundaland) are now known and comprise the East Malaya-IndoChina block, the Sibumasu block, the West Burma block, the SW Borneo block and the West Sumatra block (Fig. 1a). These blocks were re-assembled along suture zones that represent the Tethyan ocean and were attached to South China (Fig. 1a). The Inthanon suture zone in Thailand and the Bentong-Raub suture zone in Peninsular Malaysia represent the main Paleo-Tethys ocean basin (Wang et al., 2018) and the Shan Boundary suture zone in Myanmar represents Neo-Tethyan relics (Wang et al., 2018). The Sibumasu block to the west of the Bentong-Raub suture was derived from Gondwana in the late Early Permian during the opening of the Meso-Tethys (Metcalf, 2013a).

Granitoids are widely distributed in SE Asia and form three main belts (Zaw, 1990;

Schwartz et al., 1995; Gardiner et al., 2016; Searle et al., 2016; Ng et al., 2017): the Western province or Mogok-Mandalay-Mergui belt (central Myanmar and Thailand), the Main Range granitoid province (eastern Myanmar, western Thailand, western Malaysia peninsula and tin island in Indonesia) and the Eastern granitoid province (central Thailand and eastern Malay peninsula) (Fig. 1b). These granitoids were emplaced in the Late Permian, Late Jurassic, Late Cretaceous-Eocene and Paleogene (Ng et al., 2015b, 2017; Searle et al., 2016; Qian et al., 2017).

The extensive tin mineralization in southern Myanmar, Peninsular Malaysia and Tin Island (Fig. 1b) is thought to be temporally and genetically related to so-called tin granites. These granites have relatively high K₂O, SiO₂, Rb, Th and Sn, and low FeO, CaO, Na₂O, MgO, Ba and Sr contents (Schwartz et al., 1995; Ng et al., 2015a; Htun et al., 2017). The tin ore bodies generally occur either within granitic plutons or along contact zones between granitoids and sedimentary rocks and form a variety of ore deposit types including vein-, skarn- and pegmatite- and breccia-types (Linnen and Williams-Jones, 1995; Schwartz et al., 1995; Suwimonprecha et al., 1995; Htun et al., 2017). Hydrothermal vein-type deposits are the most abundant and constitute 62% of all known primary tin deposits. Skarn-, pegmatite- and breccia-types account for 24%, 12% and 1% of total known primary tin reserves, respectively (Schwartz et al., 1995).

2.2 Geology of Peninsular Malaysia

Peninsular Malaysia is a metallogenically important part of SE Asia and consists of the Western Belt, Central Belt and Eastern Belt (Fig. 2). The Western Belt in the Sibumasu block (Fig. 1a) is composed of crystalline basement overlain by middle

Cambrian to Cretaceous strata (Lee, 2009). The Eastern Belt comprises Mesoproterozoic basement overlain by fossiliferous Late Carboniferous to Triassic limestones, sandstones, shales, and volcanic rocks (Metcalf, 2013b). The Eastern Belt is thought to form part of the IndoChina- East Malaya Block that was separated from Gondwana in the Early Devonian (Usuki et al., 2013). It also has been proposed that the Eastern Belt, referred to as the East Malayan Block, was later separated from the IndoChina Block by Late Mesozoic and Cenozoic rifting in the Gulf of Thailand (Metcalf, 2013b). The Central Belt, which is composed of lineaments of serpentinite and deep-marine sedimentary rocks, has been interpreted to represent remnants of the Paleotethyan suture zone (Metcalf, 2013b; Wang et al., 2018).

The numerous granitoids in the Western Belt are considered to constitute the Main Range granitoid province, whereas those in the Eastern Belt are considered to make up the Eastern granitoid province of (Fig. 1b). Granites in the Eastern Belt have U-Pb ages ranging from 289 to 220 Ma, whereas those from the Western Belt have U-Pb ages of 227 to 201 Ma (Ng et al., 2015b).

The tin mineralization is largely concentrated within the Western Belt and Eastern Belt where it has a close spatial relationship with the granites (Hosking, 1973; Rajah et al., 1977; Schwartz and Askury, 1990). There are three types of primary tin mineralization in Peninsular Malaysia (Hutchison, 1988b): (1) vein-type, (2) skarn-type which can be subdivided into stanniferous and stanniferous-iron sub-types, and (3) tin-bearing pegmatites and aplites. Hydrothermal vein-type mineralization is ubiquitous, whereas stanniferous-iron skarns were found mainly within the Eastern Belt,

stanniferous skarns are restricted to the Western Belt and tin-bearing pegmatites and aplites are present mainly in the Western Belt (Fig. 2). (Fig. 2). This study focuses on the vein- and skarn-type tin deposits.

Skarn-type tin deposits were subdivided into stanniferous-iron and stanniferous groups by Hosking (1973). Stanniferous-iron skarns are closely associated with stanniferous calc-silicate skarn zones (Fig. 3a). There, fine-grained cassiterite is intimately associated with magnetite (Fig. 4c). The main ore bodies are crosscut by numerous quartz veins containing cassiterite, pyrite and fluorite (Fig. 4d) and the most important of them are hosted in limestone, where they occur as stanniferous veins and pipe-like bodies. The ore minerals are cassiterite, stannite, arsenopyrite, pyrite, pyrrhotite, molybdenite and bornite, and the gangue minerals are tremolite, fluorite and fluoborite (Hutchison, 1988a). Cassiterite occurs in layers parallel to the borders of the veins and pipes, and interstitial to arsenopyrite in the main body.

Cassiterite-bearing quartz veins are mostly hosted in metasedimentary rocks and locally within granites. The ore minerals are cassiterite and minor chalcopyrite, pyrrhotite and arsenopyrite (Figs. 3 and 4). Tungsten is spatially associated with the tin mineralization, commonly as wolframite (Fig. 4a). The main gangue minerals are quartz, tourmaline and muscovite (Figs. 4a, b).

3. Sampling and analytical methods

3.1 LA-ICP-MS cassiterite U-Pb dating

Nine cassiterite samples were collected from six tin deposits (Sintok, Rahman, Bandi, Setahum, Lembing and Cherul) (Table 1 and Fig. 2). Cassiterite crystals examined

in this study were separated from bulk ore samples using conventional rock crushing down to 200 μm , followed by heavy liquid and magnetic separation techniques. Selected cassiterite crystals were then mounted in epoxy resin and polished. Cathodoluminescence (CL) and backscattered electron (BSE) images were taken of each cassiterite grain and were used to examine the internal structure and guide the U-Pb geochronology.

The U-Pb isotope analyses were carried out with LA-ICP-MS at the State Key Laboratory of Ore Deposit Geochemistry, Institute of Geochemistry, Chinese Academy of Sciences (IGCAS). The system consists of an Agilent 7900 ICP-MS coupled with a 193 nm Arf excimer laser. A laser spot of 60 μm in diameter was used with an energy density on the cassiterite surface of about 4 J/cm^2 and a repetition frequency of 6 Hz. Helium gas carrying the ablated sample aerosol was mixed with argon carrier gas and nitrogen as additional diatomic gas to enhance sensitivity and flow into the ICP. An in-house cassiterite standard, AY-4, was used as an isotopic calibration standard. This standard is from the No. 19 skarn ore-body in the Anyuan Sn deposit, South China, and has been well studied using isotope dilution-thermal ionization mass spectrometry (ID-TIMS). It has a U-Pb age of 158.2 ± 0.4 Ma (Yuan et al., 2011). This cassiterite standard, which has a very low common lead concentration was analyzed twice for every five analyses of samples. Each spot analysis incorporated a background acquisition of approximately 20 s followed by 40 s of sample data acquisition. The analytical procedure is similar to that described by (Zhang et al., 2017a,b). Raw data reduction was performed off-line using ICPMSDataCal software (Liu et al., 2010).

As a test of the procedure, we analyzed cassiterite grains from the Dachang tin deposit, South China; the U-Pb ratios were calibrated against bracketing analyses of standard AY-4. We obtained an $^{206}\text{Pb}/^{238}\text{U}$ age of 90.0 ± 3.6 Ma, in agreement with previously determined ages for the Sn mineralization of 91.5 ± 2.3 Ma and 91.2 ± 1.8 Ma (Guo et al., 2018). This confirms that the method described above can be used to produce precise and accurate Pb/U ages from cassiterite.

3.2 Zircon U-Pb dating and trace element analysis

Tin-bearing (samples CR-1 and SK-10) and barren granites (sample KT-4) were sampled from Peninsular Malaysia (Fig.2 and Table .1); the samples are fresh. Zircon crystals were separated from these samples using conventional density and magnetic techniques, followed by hand-picking under a binocular microscope. The selected zircon crystals were mounted in epoxy and polished down to near half sections to expose their internal structures. An optical microscope was used to image these zircon crystals under transmitted and reflected light. Cathodoluminescence (CL) images were taken using a JXA8530F-plus electron microprobe at IGCAS. These images were used to target spot analyses for trace element and U-Pb isotopic measurements, which were conducted using LA-ICP-MS at IGCAS. A laser spot of $44 \mu\text{m}$ in diameter with an energy density on the sample surface of about $4 \text{ J}/\text{cm}^2$ and a repetition frequency of 6 Hz was used in the analyses. The U-Pb isotope and trace element analyses were carried out simultaneously. The standard NIST 610, was used as an external standard, and ^{91}Zr of 489,700 ppm as an internal standard for trace elements analyses. Zircon 91500 was used as the external standard for the U-Pb dating, and zircon GJ-1 was analyzed as an

unknown to monitor the data quality. The analytical procedures and conditions have been described by [Liu et al. \(2010\)](#). Trace element concentrations and U-Pb ages were determined using ICPMSDataCal software ([Liu et al., 2010](#)). Concordia diagrams and weighted mean calculations were made using Isoplot 4.15 ([Ludwig, 2008](#)).

3.3 Zircon Hf isotope analysis

Sample mounts were re-polished and Lu-Hf isotope analyses were performed at sites on the zircon crystals close to those analyzed for their U-Pb isotope and trace element compositions. The Lu-Hf isotope analyses were carried out at IGCAS using a Nu Plasma III multi-collector ICPMS equipped with a 193 nm Resonetics RESOLUTION S-155 laser ablation system (LA-MC-ICP-MS). Helium was used as the carrier gas to efficiently transport the aerosol to the MC-ICP-MS. Five standard zircons (GJ-1, 91500, Plešovice, Mud Tank, Penglai) were analyzed for every twenty unknown samples and one standard zircon (Penglai) for every five samples for the purpose of quality control. The analytical procedures are described in [Hu et al. \(2012\)](#). Off-line selection and integration of the analytical signal, and mass bias calibrations were performed using ICPMSDatacal ([Liu et al., 2010](#)).

4. Analytical results

4.1 Cassiterite U-Pb ages

The results of U-Pb isotope analyses for nine cassiterite samples from the Sintok, Rahman, Bandi, Setahum, Lembing and Cherul tin deposits are presented in [Appendix A](#). The ages were calculated from $^{206}\text{Pb}/^{238}\text{U}$ intercept ages for the selected crystals at the 95% confidence level using Isoplot 4.15 ([Ludwig, 2008](#)).

Cassiterite from the Cherul tin deposit yielded $^{206}\text{Pb}/^{238}\text{U}$ ages of 285.3 ± 8.5 Ma (MSWD = 1.1) for sample CR-2, and 281.3 ± 3.5 Ma (MSWD = 1.2) for sample CR-3 (Figs. 5a and b). These two ages are identical within the reported uncertainty.

Cassiterite for samples LM-1 and LM-2 from the southern part of the Lembing tin deposit have $^{206}\text{Pb}/^{238}\text{U}$ ages of 282.7 ± 4.6 Ma (MSWD = 1.0), and 282.1 ± 9.4 Ma for sample LM-2 (Figs. 5c and d). Cassiterite sample LM-6 from the northern part of the Lembing tin deposit has a U-Pb age of 284.7 ± 5.4 Ma (MSWD = 1.4) (Fig. 5e). Cassiterite sample BD-4 from a stanniferous-iron skarn ore in the Setahum deposit has a U-Pb age of 270.6 ± 4.6 Ma (MSWD = 0.7) (Fig. 5f).

Twenty-five spots were analyzed on cassiterite crystals from ore sample BD-5 collected from the Bandi deposit. The ratios of $^{206}\text{Pb}/^{238}\text{U}$, $^{207}\text{Pb}/^{235}\text{U}$, and $^{207}\text{Pb}/^{206}\text{Pb}$ vary from 0.0334 to 0.0809, 0.2591 to 5.4809, 0.0559 to 0.6186, respectively. These analytical spots record a $^{206}\text{Pb}/^{238}\text{U}$ age of 213.1 ± 3.9 Ma (MSWD = 1.1) (Fig. 5g).

Thirty-four spots were analyzed on 20 cassiterite crystals from sample RM-7 collected from the Rahman tin deposit. The ratios of $^{206}\text{Pb}/^{238}\text{U}$, $^{207}\text{Pb}/^{235}\text{U}$, and $^{207}\text{Pb}/^{206}\text{Pb}$ vary from 0.0329 to 0.5647, 0.3108 to 62.6119, 0.0717 to 0.9908, respectively. These cassiterite analyses yielded a $^{206}\text{Pb}/^{238}\text{U}$ intercept age of 226.8 ± 7.6 Ma (MSWD = 1.1) (Fig. 5g).

Thirty analyses of 25 cassiterite crystals from ore sample SK-4 of the Sintok tin deposit yielded ratios of $^{206}\text{Pb}/^{238}\text{U}$, $^{207}\text{Pb}/^{235}\text{U}$, and $^{207}\text{Pb}/^{206}\text{Pb}$ from 0.0328 to 0.0407, 0.2605 to 1.2107, 0.0574 to 0.6633, respectively. These analyses yielded a $^{206}\text{Pb}/^{238}\text{U}$ intercept age for the cassiterite of 218.9 ± 3.4 Ma (MSWD = 1.3) (Fig. 5g).

4.2 Zircon U-Pb ages

Zircon crystals from tin-bearing granite sample (CR-1) of the Cherul tin deposit in eastern Peninsular Malaysia are euhedral and colorless, but display oscillatory zoning in CL images. They locally contain inherited cores and mineral inclusions. The U-Pb age and isotope results for these crystals are reported in [Table 2](#). Eighteen analyses of 16 crystals showed that the zircon contains 82.4 ppm to 515 ppm Th and 181 ppm to 2446 ppm U and that the high Th/U ratios vary from 0.18 to 0.58. These zircon crystals produced a Concordia age of 276.0 ± 1.0 (MSWD = 0.4) Ma and a weighted mean $^{206}\text{Pb}/^{238}\text{U}$ age of 276.0 ± 1.9 Ma (MSWD = 0.2) ([Fig. 5j](#)), which are identical to the cassiterite U-Pb ages within the reported uncertainty. However, the inherited cores record much older $^{206}\text{Pb}/^{238}\text{U}$ ages of 1794 ± 17 Ma and 1783 ± 27 Ma ([Table 2](#)).

Zircon crystals from tin-bearing granite sample (SK-10) of the Sintok deposit have Th and U concentrations of 169 to 703 ppm and 483 to 3061 ppm, respectively, and high Th/U ratios (0.07 to 0.54) ([Table 2](#)). These crystals generated a Concordia age of 221.9 ± 0.6 (MSWD = 0.5) Ma and a weighted mean $^{206}\text{Pb}/^{238}\text{U}$ age of 222.0 ± 1.1 Ma (MSWD = 1.1) ([Fig. 5k](#)), which is identical to the cassiterite U-Pb age of 218.9 ± 3.4 Ma within the reported uncertainty.

Zircon crystals from a barren granite (KT-4) away from tin deposits contain 483 to 1644 ppm Th and 1201 to 3819 ppm U, corresponding to Th/U ratios of 0.32 to 0.48 ([Table 2](#)). They yielded a Concordia age of 260.5 ± 0.7 (MSWD = 2.7) Ma and a weighted mean $^{206}\text{Pb}/^{238}\text{U}$ age of 260.6 ± 1.3 Ma (MSWD = 0.6) ([Fig. 5m](#)).

4.3 The Hf isotopic composition of zircon

Zircon crystals from tin-bearing granites have similar $\varepsilon_{\text{Hf}}(t)$ values of -4.6 to -9.3 and an average of -6.4 ± 1.9 for CR-1, -3.2 to -7.8 and -5.3 ± 1.9 for SK-10 calculated using corresponding U-Pb ages, and Proterozoic two-stage Hf model age (T_{DM2}) (1.4 to 1.8 Ga for CR-1, 1.4 to 1.7 Ga for SK-10) (Table 2). In contrast, zircon crystals from the barren granite sample (KT-4) have higher and more variable $\varepsilon_{\text{Hf}}(t)$ values (-5.4 to +3.6; 0.5 ± 1.9 on average) and younger T_{DM2} ages (1.0 to 1.6 Ga) than those of the tin-bearing granites (Figs. 6a and b).

4.4 Zircon trace element chemistry

The trace elements compositions of zircon from the tin-bearing and barren granites are reported in Table 3. Zircon crystals from the tin-bearing granites have similar trace elements concentrations and variable Th/U and Sm/Yb ratios, and Hf concentrations (Fig. 7). In contrast, zircon crystals from the barren granites have homogenous trace element concentrations. The Th/U and Sm/Yb ratios, and Hf contents of these crystals concentrate in a narrow field (Fig. 7). The chondrite-normalized REE profiles of the zircon are broadly similar with positive Ce anomalies, negative Eu anomalies, and a strong enrichment of the HREE in all samples. Both the texture and chemistry are consistent with a magmatic origin, and thus zircon chemistry records the physicochemical conditions of granite formation.

4.5 Ti-in-zircon thermometry and zircon $\text{Ce}^{4+}/\text{Ce}^{3+}$ ratios

The temperature of granite crystallization was estimated using the Ti-in-zircon geothermometer (Ferry and Watson; 2007), assuming an activity of SiO_2 of 1 (quartz

saturation and a TiO_2 activity of 0.63 because rutile has not been observed in these granites. Temperatures so-estimated for tin-bearing granites associated with the the Cheril and Sintok tin deposits (CR-1 and SK-10) ranged from X-Y and W-Z, respectively, although they were mostly between 700 °C and 800 °C (Table 3, Fig. 7). In contrast, the temperatures estimated for a barren granite (sample KT-4) are mostly between 590 °C and 689 °C, and thus somewhat lower than those of the tin-bearing granites (Fig. 7) and (Table 3).

The $\text{Ce}^{4+}/\text{Ce}^{3+}$ ratios of zircon from the tin-bearing and barren granites referred to in the previous paragraph were estimated from zircon-melt partition coefficients for Ce^{3+} and Ce^{4+} , which were calculated using the lattice strain model and the whole rock concentrations of the REE and other HFSE (Zr, Hf, U, and Th) as a proxy for the melt and the concentrations of these elements in zircon (Table 3) (Blundy and Wood, 1994; Ballard et al., 2002). The calculated $\text{Ce}^{4+}/\text{Ce}^{3+}$ ratios of zircon from the tin-bearing granites are mostly between 4 to 67 (Table 3), whereas those of zircon from the barren granites are mostly higher than 40 (Table 3).

5. Discussion

A reliable geochronological framework for tin mineralization in Peninsular Malaysia has not been available because the age of tin mineralization has been inferred from the ages of the associated granites and not determined directly. Moreover, the factors controlling granite-related tin mineralization in Peninsular Malaysia are unclear. The U-Pb dates reported for cassiterite in this study suggests that there were two main tin mineralizing events in Peninsular Malaysia, i.e., between 290

and 270Ma and between 230 and 210 Ma. The $\varepsilon_{\text{Hf}}(t)$ values and $\text{Ce}^{4+}/\text{Ce}^{3+}$ ratios of zircons from tin-bearing granites are different from those of barren granites. It is indicated that magmatic source and redox state controlled the development of tin-fertile magmas leading to magmatic hydrothermal tin deposits. The two-periods important tin mineralization and related granites in Peninsular Malaysia occurred at a special tectonic setting and was closely related to Paleo-Tethyan evolution.

5.1 Geochronological framework of tin mineralization

It is well known that extensive tin mineralization occurred in Peninsular Malaysia (Hosking, 1973; Rajah et al., 1977). In recent years, the tin mineralization was thought to occur mainly between 227 and 201 Ma, inferred from U-Pb ages of zircon (Ng et al., 2015b). However, the precise ages of tin metallogenesis were not reported and remain obscure. Cassiterite is a main ore mineral in all tin deposits and in principle contains high U and typically low common Pb, with a high Pb closure temperature of 300 to 450 °C (Zhang et al., 2011). Cassiterite is thus potentially suitable for U-Pb dating and is increasingly used to directly date tin deposits (Yuan et al., 2008, 2011; Zhang et al., 2017a; Liu et al., 2018).

Nine cassiterite samples were taken from the vein- and skarn-type tin deposits in the Western Belt and Eastern Belt (Fig. 2). The results reveal that the Sintok, Rahman, Bandi, Setahum and Lembing and Cherul tin deposits formed at 281.9 ± 3.4 Ma, 226.8 ± 7.6 Ma, 213.1 ± 3.9 Ma, 270.6 ± 4.6 Ma, 282.7 ± 4.6 Ma and 281.3 ± 8.5 Ma, respectively (Figs. 6a-i). These cassiterite U-Pb ages fall in two ranges of 230 - 210 Ma and 290 - 270 Ma (Fig. 8a). For any individual deposit, zircon from tin-bearing granites

has U-Pb ages that coincide well with cassiterite U-Pb ages within uncertainty (e.g., Sintok: 276.0 ± 1.0 Ma, Cherul: 222.0 ± 1.1 Ma) (Figs. 5j and k). In the light of zircon U-Pb ages from literatures and our unpublished data, we observed that granite with U-Pb ages of 230 - 210 Ma and 290 - 270 Ma also took place at Peninsular Malaysia (Fig. 8b). Thus, we infer that two important granite-related tin mineralization may occur at 230 - 210 Ma and 290 - 270 Ma in Peninsular Malaysia. In addition, stable isotopes (H and O) of ore-forming fluids in tin deposits point to magmatic fluids (Linnen, 1998). Thus, tin mineralization may occur and were spatiotemporally and genetically related to granites in Peninsular Malaysia.

5.2 Controls of magmatic source on tin mineralization

There is a general consensus that the tin mineralization is spatially, temporally and genetically related to granite. However, the key factors controlling this relationship is still strongly debated. Some researchers have expressed the view that the source of the granitic magma was the determining factor for the formation of the deposits (Taylor, 1979; Romer and Kroner, 2015; Romer and Kroner, 2016). The other workers highlighted that magmatic evolution plays key role in forming tin deposits (Lehmann and Harmanto, 1990; Lehmann, 1990).

Our samples from tin-bearing and barren granites all are highly evolved with SiO₂ contents from 70 wt% to 76 wt%. They have very similar Sn contents and there is no correlation between SiO₂ and Sn contents (Table 3). However, the tin-bearing granites can be distinguished from the barren granites by their lower $\epsilon_{\text{Hf}}(t)$ values for zircon (-4.6 to -9.3 versus -5.4 to +3.6) (Figs. 7a and c) The two-stage Hf model ages ($T_{\text{DM}2}$) of

the tin-bearing granites are also older than the barren granites (Fig. 6b). The Hf isotopic composition of zircon from tin-bearing granites and is similar to that of the Paleo- to Meso-Proterozoic crustal basement (Fig. 9a). This indicates that the tin-bearing granites have the same provenance and could have been derived from partial melting of Paleo- to Meso-Proterozoic crust. In contrast, the barren granites have highly variable zircon $\varepsilon_{\text{Hf}}(t)$ values (-5.4 to +3.6). The involvement of a mantle components has been suggested as a means of producing such inhomogeneous zircon Hf isotope ratios in granite (Kemp et al., 2007; Yang et al., 2007). Compared to mantle-derived magmas, ancient crust is rich in rare-metal such as Sn (Rudnick and Gao, 2003; Romer and Kroner, 2015). Thus, Sn-rich ancient crust-derived magmas may provide necessary sources of granite-related tin mineralization.

5.3 Reduction state inherited from magmatic sources

Tin has oxidation states of 2^+ and 4^+ at geologically relevant conditions and the transition from Sn^{2+} -dominant to Sn^{4+} -dominant valences occurs over a narrow range of f_{O_2} (FMQ+1.0 to FMQ+2.0) (Linnen et al., 1996). At reduced conditions, tin is highly soluble because of its occurrence as the Sn^{2+} species, whereas at oxidized conditions it is relatively insoluble because of the dominance of Sn^{4+} species (Linnen et al., 1996). Thus, the redox state of the magmas is generally taken as a critical parameter for the genesis of tin deposits (Linnen et al., 1995, 1996).

We employed the $\text{Ce}^{4+}/\text{Ce}^{3+}$ ratio of the zircon reported earlier to estimate the oxygen fugacity of the magmas producing the tin granites considered in this study using the methods of Smythe and Brenan (2015). In this method, oxygen fugacity

depends on water content, melt composition, the Ce^{4+}/Ce^{3+} ratio of the melt and temperature. The Ce^{4+}/Ce^{3+} ratio of magma was calculated as described earlier from the zircon-melt partition coefficients for Ce^{4+} and Ce^{3+} and the temperature was taken to be that obtained using the Ti-in-zircon geothermometer. The water content of the magmas was assumed to be 6.5%, because rare-metal mineralized peraluminous magmas are typically water-rich (the H_2O content varies between 6.5 and 8.5% based on experimental studies in haplo-granite system; Holtz et al., 2001). The oxygen fugacity so calculated for the Cherul pluton (CR-1) is equivalent to $\Delta FMQ-3.4$ and that for the Sintok pluton (SK-10) is equivalent to $\Delta FMQ-1.8$ (Fig. 7c). These values indicate that tin-granites crystallize from highly reduced magmas, an observation that is consistent with their relatively low zircon Ce^{4+}/Ce^{3+} ratios; the generally higher zircon Ce^{4+}/Ce^{3+} ratios of the barren granites suggest that their magmas were more oxidising (Fig. 6c and d)..

To determine when and how a tin-mineralized magma becomes reduced, it is essential to identify the factors that control Sn enrichment. The Hf contents of zircon from both the tin-bearing and barren granites increase with increasing temperature as determined using Ti-in-zircon thermometry (Fig. 7b), and with the zircon Ce^{4+}/Ce^{3+} ratio (Fig. 7d). This implies that magma evolution affected the redox state. However, the zircon Ce^{4+}/Ce^{3+} ratio and oxygen fugacity of the tin mineralized magma are generally lower than those of barren granitic magmas. Zircon Ce^{4+}/Ce^{3+} ratios are positively correlated with $\epsilon_{Hf}(t)$ values (Fig. 6c) and negatively correlated with T_{DM2} ages (Fig. 7a). These features indicate that the reduced mineralized magmas were

dominantly inherited from the source with only a minor effect on magmatic evolution.

Under reduced conditions, Sn occurs dominantly as Sn²⁺ and can be effectively transferred into magmas during partial melting.

5.4 Tin metallogeny during the evolution of Paleo-Tethyan

Tin deposits in Peninsular Malaysia formed episodically in the east Paleo-Tethyan system. The tin-bearing granites have similar magmatic sources and redox states, which differ from those of barren granites. The formation of tin deposits could be linked to Paleo-Tethyan evolution.

The Paleo-Tethyan evolution from subduction to collision and assembly of continental fragments has been addressed in several studies ([Metcalf, 2013a](#); [Searle et al., 2016](#); [Wang et al., 2018](#)). Estimates of the timing of oceanic closure in the east Paleo-tethyan domain range from Permian to late Triassic and even Jurassic ([Searle et al., 2012](#); [Metcalf, 2013b, a](#); [Ng et al., 2015a, b](#); [Wang et al., 2016](#); [Qian et al., 2017](#)). Arc magmatism along or between the Changning-Menglian-Inthanon-Bentong-Raub suture zone occurred between 289 and 240 Ma ([Sevastjanova et al., 2011](#); [Ng et al., 2015b](#); [Wang et al., 2018](#)). The youngest arc-related granites in the Inthanon areas have an age of ~240 Ma (e. g., [Zaw and Meffre, 2007](#), [Gardiner et al., 2016a, b](#), [Wang et al., 2018](#)). High-Mg andesite, dacite, basaltic andesite and monzonite porphyry from the Loei and Lincang-Sukhothai areas formed in a supra-subduction zone, and have been dated at ~249-241 Ma (e.g., [Kamvong and Zaw, 2009](#), [Wang et al., 2010](#), [Qian et al., 2016](#)). Igneous rocks in the Lincang, Sukhothai, East Malaya belts have an age peaks around 237 Ma, and are interpreted as the syn-collisional magmatic products

(Wang et al., 2016, 2018; Qian et al., 2017). Radiolarian assemblages along the Changning-Menglian-Inthanon-Bentong-Raub suture zone indicate that the accretion of Paleo-Tethyan seamounts and the final closure of the Paleo-Tethyan Ocean occurred at ~247 Ma and ~240 Ma, respectively (Ueno, 1999, 2003, Metcalfe, 2002, 2013a, Ito et al., 2016). Thus, a transition from subduction of the Paleo-Tethyan Ocean to the collision of the Sibumasu block with East Malaysia-IndoChina blocks may occur at ~240 Ma (Figs. 9b and 10). Following the closure of Paleo-Tethyan Ocean, the 240-230 Ma granitoids show high positive to negative $\epsilon_{\text{Hf}}(t)$ (-15 to +10) and $\epsilon_{\text{Nd}}(t)$ (-12 to +4) values, suggestive of a significant involvement of a juvenile component for the origin of these granitoids (Wang et al., 2018). These granitoids are widespread in SE Asia and interpreted as the products of syn-collisional magmatism (Wang et al., 2018) (Figs. 9b and 10).

Barren granites from the East Belt of Peninsular Malaysia have U-Pb ages of 245-265 Ma and positive zircon $\epsilon_{\text{Hf}}(t)$ values and relatively young T_{DM2} Hf model ages (Fig.9b). The 255-246 Ma calc-alkaline I-type granites (e.g., Baimaxueshan, Xin'anzhai and Phia Bioc) and mafic-intermediate rocks (e.g., Maoheshan basalt and Muong Lay diorite) along the Jinshanjiang-Ailaoshan and Song Ma suture zones also have high $\epsilon_{\text{Hf}}(t)$ and $\epsilon_{\text{Nd}}(t)$ values (Liu et al., 2011, 2012, 2017, Wang et al., 2016). The 245-265 Ma granitoids are thought to be related to subduction of the Paleotethys beneath the East Malaya-IndoChina block in response to the opening of the Mesotethyan Ocean (Fig. 10). These subduction-related barren granitoids crystallized from magmas having a dominantly mantle source (Wang et al., 2018); the contribution from sedimentary-

sourced melts was insignificant (Ng et al., 2015a).

Compared to the barren granites the 290-270 Ma, the zircon $\epsilon_{\text{Hf}}(t)$ values (Fig. 9) and whole-rock $\epsilon_{\text{Nd}}(t)$ values (-3.8 to -2.6) of the tin-bearing granites from the Eastern Province of Peninsular Malaysia are strongly negative (Ng et al., 2015a) and their T_{DM2} Hf model ages relatively old (Fig. 6). This indicates that these granites were likely generated from a supracrustal sediment-dominated source. Partial melting of supracrustal sedimentary rocks may have resulted from an elevated thermal gradient of crust in response to the initiation Paleo-Tethys subduction (Figs. 9b and 10). The 230-210 Ma tin-bearing granites in both the Main range and Eastern Provinces of Peninsular Malaysia also have strongly negative $\epsilon_{\text{Hf}}(t)$ values (Figs. 6 and 9) (Ng et al., 2015a), indicating that they too were produced from a supracrustal sediment-dominated source. These granites are considered to be the products of post-collisional magmatism in response to gravitational collapse of the orogenic belt during crustal extension (Schwartz et al., 1995; Ng et al., 2015b; Wang et al., 2018). Thus, the tin mineralization and associated granitic magmatism occurred during the Early Permian (290-270 Ma) and Late Triassic (230-210 Ma) in Peninsular Malaysia as a result of crustal anatexis in response to initial Paleo-Tethyan subduction and post-collision crustal extension during evolution of Paleo-Tethyan system, respectively.

6. Conclusions

(1) Cassiterite from the Sintok, Rahman, Bandi, Setahum, Lembing and Cherul tin deposits have U-Pb ages of 281.9 ± 3.4 Ma, 226.8 ± 7.6 Ma, 213.1 ± 3.9 Ma, 270.6 ± 4.6 Ma, 282.7 ± 4.6 Ma and 281.3 ± 8.5 Ma, respectively. Cassiterite U-Pb dating results

suggest that tin mineralization in Peninsular Malaysia occurred at 230 - 210 Ma and 290 - 270 Ma.

(2) The tin-bearing granites from the Cherul and Sintok intruded at 276.0 ± 1.9 Ma and 221.9 ± 0.6 Ma, respectively, which coincide with their corresponding cassiterite U-Pb ages. In contrast, the barren granites intruded at 260.5 ± 0.7 Ma and lie in the time gap between two tin mineralization periods.

(3) The tin-bearing granitic magmas were derived from partial melting of sediment-dominated ancient crust. Compared to barren granite, the tin-bearing granites are more reduced that were inherited from magma source. Thus, magmatic source and redox state controlled the propensity of granite leading to tin mineralization.

(4) The tin mineralization and associated granitic magmatism in Peninsular Malaysia resulted from crustal anatexis in response to initial Paleo-Tethyan subduction and post-collision crustal extension in the context of Paleo-Tethyan system.

Acknowledgement

This research was financially supported by National Key R&D Program of China (No. 2016YFC0600405), the National Natural Science Foundation of China (Grant No. 41673054), and a special fund managed by the State Key Laboratory of Ore Deposit Geochemistry, Chinese Academy of Sciences. We thank the geologists of China Nonferrous Metals (Guilin) Geology and Mining Co.,Ltd, especially Mr Jun-Hong Zhao for their assistance during our field work.

Figure captions

Fig. 1 Tectonic sketch map of SE Asia showing the major suture boundaries and tectonic fragments (a), and the distribution of tin deposits and granites in SE Asia (b).

Modified from previous literatures ([Hutchison, 1988a](#); [Schwartz et al., 1995](#); [Wang et al., 2018](#)).

Fig. 2 Simplified geological map of Peninsular Malaysia showing distribution of tin deposits and granites. Modified after [Hutchison \(1988a\)](#) and [Ng et al. \(2015a\)](#). Samples locations and U-Pb ages of zircon and cassiterite are shown in this map.

Fig. 3 The field photos of stanniferous-iron skarn tin deposits (a) and vein type tin deposits (b-d) in Peninsular Malaysia.

Fig. 4 Photographs of stanniferous skarn and veins showing the minerals assemblages

Fig. 5 U-Pb Concordia diagrams of cassiterite and zircon.

Fig. 6 Plots of U-Pb ages (Ma) versus $\epsilon_{\text{Hf}}(t)$ values (a), U-Pb ages (Ma) versus T_{DM2} ages (b), $\epsilon_{\text{Hf}}(t)$ values versus $\text{Ce}^{4+}/\text{Ce}^{3+}$ ratios (c), and U-Pb ages (Ma) versus $\text{Ce}^{4+}/\text{Ce}^{3+}$ ratios (d) for zircon from both tin mineralized and barren granites.

Fig. 7 Plots of T_{DM2} ages versus $\text{Ce}^{4+}/\text{Ce}^{3+}$ ratios (a), Ti-in-zircon thermometry versus Hf concentrations (b), magmatic oxygen fugacity (c), and $\text{Ce}^{4+}/\text{Ce}^{3+}$ ratios versus Hf concentrations (d) based on zircon from both tin mineralized and barren granites.

Fig. 8 Histograms of cassiterite U-Pb ages (a) and zircon U-Pb ages (b) from Peninsular Malaysia.

Fig. 9 Plots of formation age (Ma) versus $\epsilon_{\text{Hf}}(t)$ values for the Paleotethyan-related granitoids from Peninsular Malaysia. The tin-bearing granites have similar $\epsilon_{\text{Hf}}(t)$

values and were related to special tectonic setting during Paleoththyan evolution. The evolution of depleted mantle with present-day $^{176}\text{Lu}/^{177}\text{Hf} = 0.0384$ and $^{176}\text{Hf}/^{177}\text{Hf} = 0.28325$ (Griffin et al., 2000). Chondrite with present-day $^{176}\text{Lu}/^{177}\text{Hf} = 0.0332$ and $^{176}\text{Hf}/^{177}\text{Hf} = 0.282772$, continental upper crust and lower crust with present-day $^{176}\text{Lu}/^{177}\text{Hf} = 0.0093$ and 0.022 , respectively (Wu et al., 2007) and references therein). The corresponding lines of new-crustal generation are calculated by assuming the $^{176}\text{Lu}/^{177}\text{Hf}$ ratio of 0.015 for the averaged continental crust (Griffin et al., 2000).

Fig. 10 Schematic tectonic cartons showing the Paleo-Tethyan evolution in Peninsular Malaysia. The two tin mineralization events and associated granite magmatism in Peninsular Malaysia as a result of crustal anatexis in respond to initial Paleo-Tethyan subduction and post-collision crustal extension.

Tables

Table 1 Samples locations and U-Pb ages of cassiterite and zircon

Table 2 Zircon U-Pb and Lu-Hf isotopes of both tin-bearing and barren granites

Table 3 Zircon trace element and calculated parameter

Appendix

Appendix A U-Pb dating of nine cassiterite samples from six deposits analyzed by LA-ICP-MS single spot-analysis

References

- Ballard, J. R., Palin, M. J., and Campbell, I. H., 2002, Relative oxidation states of magmas inferred from Ce (IV)/Ce (III) in zircon: application to porphyry copper deposits of northern Chile: *Contributions to Mineralogy and Petrology*, v. 144, p. 347-364.
- Blundy, J., and Wood, B., 1994, Prediction of crystal-melt partition coefficients from elastic moduli: *Nature*, v. 372, p. 452-454.
- Ferry, J. M., and Watson, E. B., 2007, New thermodynamic models and revised calibrations for the Ti-

- in-zircon and Zr-in-rutile thermometers: *Contributions to Mineralogy and Petrology*, v. 154, p. 429-437.
- Gardiner, N. J., Robb, L. J., Morley, C. K., Searle, M. P., Cawood, P. A., Whitehouse, M. J., Kirkland, C. L., Roberts, N. M. W., and Myint, T. A., 2016, The tectonic and metallogenic framework of Myanmar: A Tethyan mineral system: *Ore Geology Reviews*, v. 79, p. 26-45.
- Griffin, W. L., Pearson, N. J., Belousova, E., Jackson, S. E., van Achterbergh, E., O'Reilly, S. Y., and Shee, S. R., 2000, The Hf isotope composition of cratonic mantle: LAM-MC-ICPMS analysis of zircon megacrysts in kimberlites: *Geochimica Et Cosmochimica Acta*, v. 64, p. 133-147.
- Guo, J., Zhang, R., Sun, W., Ling, M., Hu, Y., Wu, K., Luo, M., and Zhang, L., 2018, Genesis of tin-dominant polymetallic deposits in the Dachang district, South China: Insights from cassiterite U-Pb ages and trace element compositions: *Ore Geology Reviews*, v. 95, p. 863-879.
- Holtz, F., Johannes, W., Tamic, N., and Behrens, H., 2001, Maximum and minimum water contents of granitic melts generated in the crust: a reevaluation and implications: *Lithos*, v. 56, p. 1-14.
- Hosking, K., 1973, The primary tin mineralization patterns of West Malaysia, 297-308 p.
- Htun, T., Htay, T., and Zaw, K., 2017, Chapter 28 Tin-tungsten deposits of Myanmar: *Geological Society London Memoirs*, v. 48, p. 625-647.
- Hu, Z., Liu, Y., Gao, S., Liu, W., Zhang, W., Tong, X., Lin, L., Zong, K., Li, M., Chen, H., Zhou, L., and Yang, L., 2012, Improved in situ Hf isotope ratio analysis of zircon using newly designed X skimmer cone and jet sample cone in combination with the addition of nitrogen by laser ablation multiple collector ICP-MS: *Journal of Analytical Atomic Spectrometry*, v. 27, p. 1391-1399.
- Hutchison, C. S., 1988a, *Geology of Tin Deposits in Asia and the Pacific*, Springer-Verlag, 633-644 p.
- Hutchison, C. S., 1988b, The Tin Metallogenic Provinces of S.E. Asia and China: A Gondwanaland Inheritance, Berlin, Heidelberg, 1988b, *Geology of Tin Deposits in Asia and the Pacific*, p. 225-234.
- Kemp, A., Hawkesworth, C., Foster, G., Paterson, B., Woodhead, J., Hergt, J., Gray, C., and Whitehouse, M., 2007, Magmatic and crustal differentiation history of granitic rocks from Hf-O isotopes in zircon: *Science*, v. 315, p. 980-983.
- Lehmann, B., and Harmanto, 1990, Large-scale tin depletion in the Tanjungpandan tin granite, Belitung Island, Indonesia: *Economic Geology*, v. 85, p. 99-111.
- Lehmann, B., Jungyusuk, N., Khositanont, S., Höhndorf, A., and Kuroda, Y., 1994, The tin-tungsten ore system of Pilok, Thailand: *Journal of Southeast Asian Earth Sciences*, v. 10, p. 51-63.
- Lehmann, P. D. B., 1990, *Metallogeny of Tin*, Springer Berlin Heidelberg.
- Linnen, R. L., 1998, Depth of emplacement, fluid provenance and metallogeny in granitic terranes: a comparison of western Thailand with other tin belts: *Mineralium Deposita*, v. 33, p. 461-476.
- Linnen, R. L., Pichavant, M., and Holtz, F., 1996, The combined effects of fO₂ and melt composition on SnO₂ solubility and tin diffusivity in haplogranitic melts: *Geochimica et Cosmochimica Acta*, v. 60, p. 4965-4976.
- Linnen, R. L., Pichavant, M., Holtz, F., and Burgess, S., 1995, The effect of fo₂ on the solubility, diffusion, and speciation of tin in haplogranitic melt at 850°C and 2 kbar: *Geochimica et Cosmochimica Acta*, v. 59, p. 1579-1588.
- Linnen, R. L., and Williams-Jones, A. E., 1995, Genesis of a magmatic metamorphic hydrothermal system; the Sn-W polymetallic deposits at Pilok, Thailand: *Economic Geology*, v. 90, p. 1148-1166.
- Liu, P., Mao, J., Santosh, M., Xu, L., Zhang, R., and Jia, L., 2018, The Xiling Sn deposit, Eastern

- Guangdong Province, Southeast China: A new genetic model from $^{40}\text{Ar}/^{39}\text{Ar}$ muscovite and U-Pb cassiterite and zircon geochronology: *Economic Geology*, v. 113.
- Liu, Y., Gao, S., Hu, Z., Gao, C., Zong, K., and Wang, D., 2010, Continental and Oceanic Crust Recycling-induced Melt–Peridotite Interactions in the Trans-North China Orogen: U–Pb Dating, Hf Isotopes and Trace Elements in Zircons from Mantle Xenoliths: *Journal of Petrology*, v. 51, p. 537-571.
- Ludwig, K. R., 2008, User's manual for Isoplot 3.70: a geochronological toolkit for Microsoft Excel, Kenneth R. Ludwig.
- Metcalfe, I., 2013a, Gondwana dispersion and Asian accretion: Tectonic and palaeogeographic evolution of eastern Tethys: *Journal of Asian Earth Sciences*, v. 66, p. 1-33.
- Metcalfe, I., 2013b, Tectonic evolution of the Malay Peninsula: *Journal of Asian Earth Sciences*, v. 76, p. 195-213.
- Ng, S. W.-P., Whitehouse, M. J., Roselee, M. H., Teschner, C., Murtadha, S., Oliver, G. J. H., Ghani, A. A., and Chang, S.-C., 2017, Late Triassic granites from Bangka, Indonesia: A continuation of the Main Range granite province of the South-East Asian Tin Belt: *Journal of Asian Earth Sciences*, v. 138, p. 548-561.
- Ng, S. W. P., Chung, S. L., Robb, L. J., Searle, M. P., Ghani, A. A., Whitehouse, M. J., Oliver, G. J. H., Sone, M., Gardiner, N. J., and Roselee, M. H., 2015a, Petrogenesis of Malaysian granitoids in the Southeast Asian tin belt: Part 1. Geochemical and Sr-Nd isotopic characteristics: *Geological Society of America Bulletin*, v. 127, p. 1209-1237.
- Ng, S. W. P., Whitehouse, M. J., Searle, M. P., Robb, L. J., Ghani, A. A., Chung, S. L., Oliver, G. J. H., Sone, M., Gardiner, N. J., and Roselee, M. H., 2015b, Petrogenesis of Malaysian granitoids in the Southeast Asian tin belt: Part 2. U-Pb zircon geochronology and tectonic model: *Geological Society of America Bulletin*, v. 127, p. 1238-1258.
- Qian, X., Feng, Q., Wang, Y., Zhao, T., Zi, J.-W., Udchachon, M., and Wang, Y., 2017, Late Triassic post-collisional granites related to Paleotethyan evolution in SE Thailand: Geochronological and geochemical constraints: *Lithos*, v. 286-287, p. 440-453.
- Rajah, S. S., Chand, F., and Singh, D. S., 1977, The granitoids and mineralization of the Eastern Belt of Peninsular Malaysia.
- Romer, R. L., and Kroner, U., 2015, Sediment and weathering control on the distribution of Paleozoic magmatic tin–tungsten mineralization: *Mineralium Deposita*, v. 50, p. 327-338.
- Romer, R. L., and Kroner, U., 2016, Phanerozoic tin and tungsten mineralization—Tectonic controls on the distribution of enriched protoliths and heat sources for crustal melting: *Gondwana Research*, v. 31, p. 60-95.
- Rudnick, R., and Gao, S., 2003, Composition of the continental crust. In: Holland, H.D., and Turekian, K.K., eds., *Treatise on Geochemistry*: Amsterdam, Elsevier, v. 3, p. 1-64.
- Schwartz, M. O., and Askury, A., 1990, Granite magmatism and tin-tungsten metallogenesis in the Kuantan–Dungun area, Malaysia.
- Schwartz, M. O., Rajah, S. S., Askury, A. K., and Putthapiban, P., 1995, The Southeast-Asian Tin Belt: *Earth-Science Reviews*, v. 38, p. 95-286.
- Searle, M. P., Robb, L. J., and Gardiner, N. J., 2016, Tectonic Processes and Metallogeny along the Tethyan Mountain Ranges of the Middle East and South Asia (Oman, Himalaya, Karakoram, Tibet, Myanmar, Thailand, Malaysia): *Society of Economic Geologists, Inc. Special Publication*, v. 19, p. 301-327.

- Searle, M. P., Whitehouse, M. J., Robb, L. J., Ghani, A. A., Hutchison, C. S., Sone, M., Ng, S., Roselee, M. H., Chung, S. L., and Oliver, J., 2012, Tectonic evolution of the Sibumasu-Indochina terrane collision zone in Thailand and Malaysia: Constraints from new U-Pb zircon chronology of SE Asian tin granitoids: *Journal of the Geological Society*, v. 169, p. 444-50.
- Sevastjanova, I., Clements, B., Hall, R., Belousova, E. A., Griffin, W. L., and Pearson, N., 2011, Granitic magmatism, basement ages, and provenance indicators in the Malay Peninsula: Insights from detrital zircon U-Pb and Hf-isotope data: *Gondwana Research*, v. 19, p. 1024-1039.
- Smythe, D. J., and Brenan, J. M., 2015, Cerium oxidation state in silicate melts: Combined fO₂, temperature and compositional effects: *Geochimica et Cosmochimica Acta*, v. 170, p. 173-187.
- Suwimonprecha, P., Cerny, P., and Friedrich, G., 1995, Rare metal mineralization related to granites and pegmatites, Phuket, Thailand: *Economic Geology*, v. 90, p. 603-615.
- Taylor, R. G., 1979, *Geology of tin deposits*, Elsevier.
- Wang, Y., He, H., Cawood, P. A., Srithai, B., Feng, Q., Fan, W., Zhang, Y., and Qian, X., 2016, Geochronological, elemental and Sr-Nd-Hf-O isotopic constraints on the petrogenesis of the Triassic post-collisional granitic rocks in NW Thailand and its Paleotethyan implications: *Lithos*, v. 266-267, p. 264-286.
- Wang, Y., Qian, X., Cawood, P. A., Liu, H., Feng, Q., Zhao, G., Zhang, Y., He, H., and Zhang, P., 2018, Closure of the East Paleotethyan Ocean and amalgamation of the Eastern Cimmerian and Southeast Asia continental fragments: *Earth-Science Reviews*, v. 186, p. 195-230.
- Wu, F.-Y., Li, X.-H., Zheng, Y.-F., and Gao, S., 2007, Lu-Hf isotopic systematics and their applications in petrology (in Chinese with English abstract): *Acta Petrologica Sinica*, v. 23, p. 185-220.
- Yang, J.-H., Wu, F.-Y., Wilde, S., Xie, L.-W., Yang, Y.-H., and Liu, X.-M., 2007, Tracing magma mixing in granite genesis: in situ U-Pb dating and Hf-isotope analysis of zircons: *Contributions to Mineralogy and Petrology*, v. 153, p. 177-190.
- Yuan, S., Peng, J., Hao, S., Li, H., Geng, J., and Zhang, D., 2011, In situ LA-MC-ICP-MS and ID-TIMS U-Pb geochronology of cassiterite in the giant Furong tin deposit, Hunan Province, South China: New constraints on the timing of tin-polymetallic mineralization: *Ore Geology Reviews*, v. 43, p. 235-242.
- Yuan, S., Peng, J., Hu, R., Li, H., Shen, N., and Zhang, D., 2008, A precise U-Pb age on cassiterite from the Xianghualing tin-polymetallic deposit (Hunan, South China): *Mineralium Deposita*, v. 43, p. 375-382.
- Zaw, K., 1990, Geological, petrological and geochemical characteristics of granitoid rocks in Burma: with special reference to the associated W-Sn mineralization and their tectonic setting: *Journal of Southeast Asian Earth Sciences*, v. 4, p. 293-335.
- Zhang, D. L., Peng, J. T., Hu, R. Z., Yuan, S. D., and Zheng, D. S., 2011, The closure of U-Pb isotope system in cassiterite and its reliability for dating: *Dizhi Lunping* (in Chinese with English abstract): *Geological Review*, v. 57, p. 549-544.
- Zhang, R., Lehmann, B., Seltnann, R., Li, C., and Sun, W., 2017a, Cassiterite U-Pb geochronology constrains magmatic-hydrothermal evolution in complex evolved granite systems: The classic Erzgebirge tin province (Saxony and Bohemia): *Geology*, v. 45, p. 1095-1098.
- Zhang, R., Lu, J., Lehmann, B., Li, C., Li, G., Zhang, L., Guo, J., and Sun, W., 2017b, Combined zircon and cassiterite U-Pb dating of the Piaotang granite-related tungsten-tin deposit, southern Jiangxi tungsten district, China: *Ore Geology Reviews*, v. 82, p. 268-284.
- USGS, 2019, U.S. Geological Survey, Mineral Commodity Summaries. Tin, p. 172-173.

Lee, C.P., 2009. Palaeozoic Stratigraphy. In: Hutchison, C.S., Tan, D.N.K. (Eds.), *Geology of Peninsular Malaysia*. University of Malaya/Geological Society of Malaysia, Kuala Lumpur, pp. 55–86.

Usuki, T., Lan, C.-Y., Wang, K.-L., Chiu, H.-Y., 2013. Linking the Indochina block and Gondwana during the Early Paleozoic: Evidence from U-Pb ages and Hf isotopes of detrital zircons. *Tectonophysics*: v. 586, p. 145–159.

Fig. 1

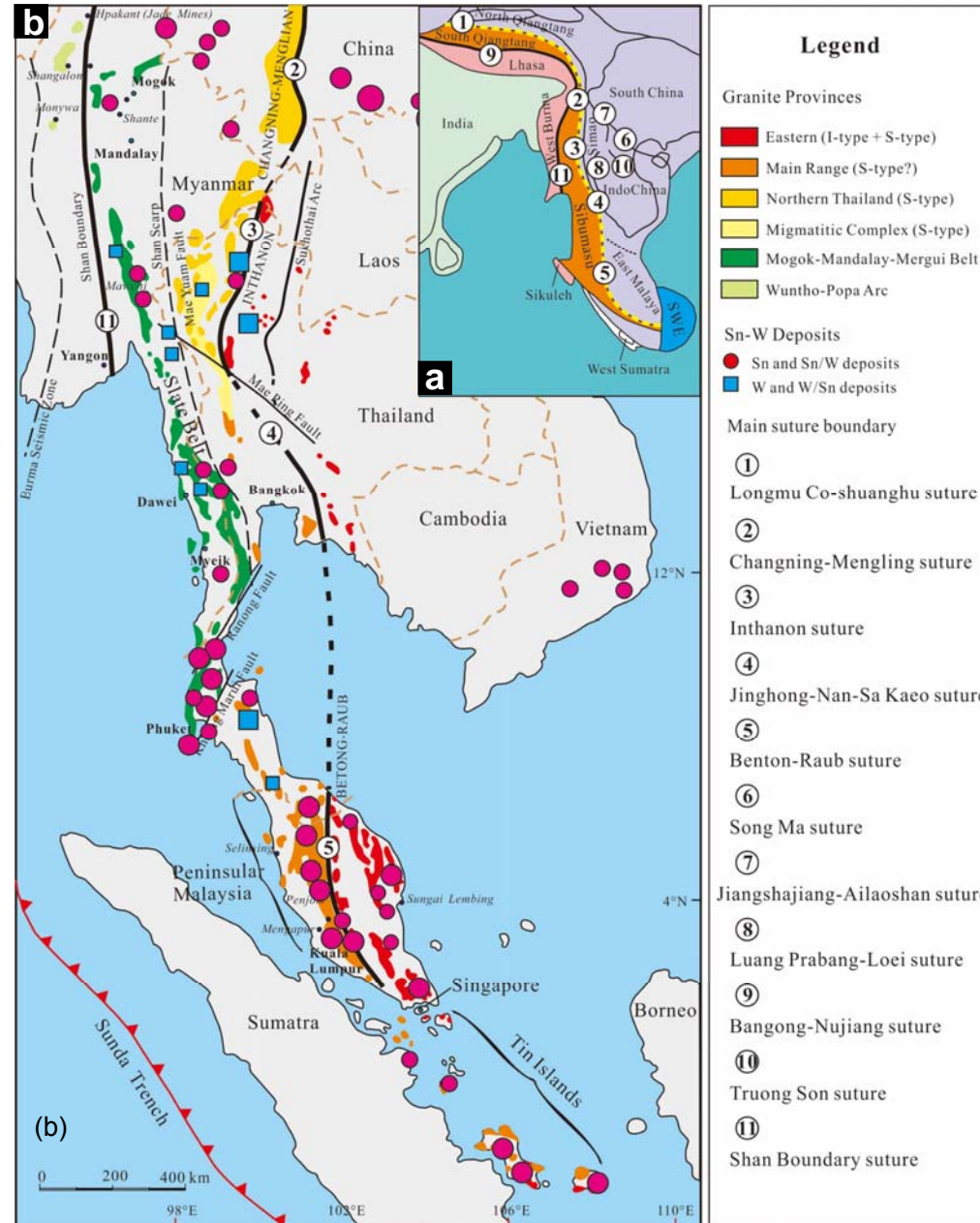


Fig. 2

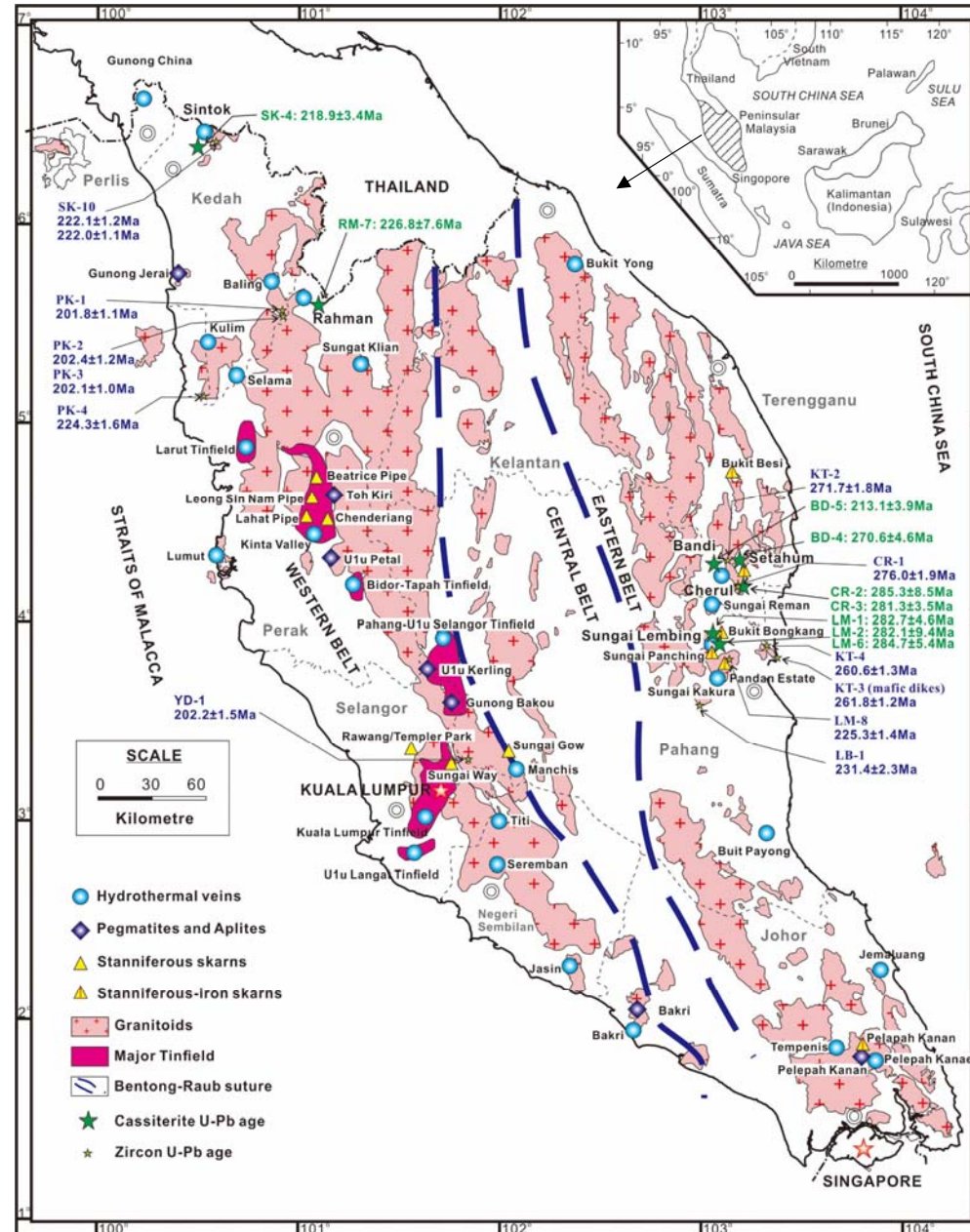


Fig. 3

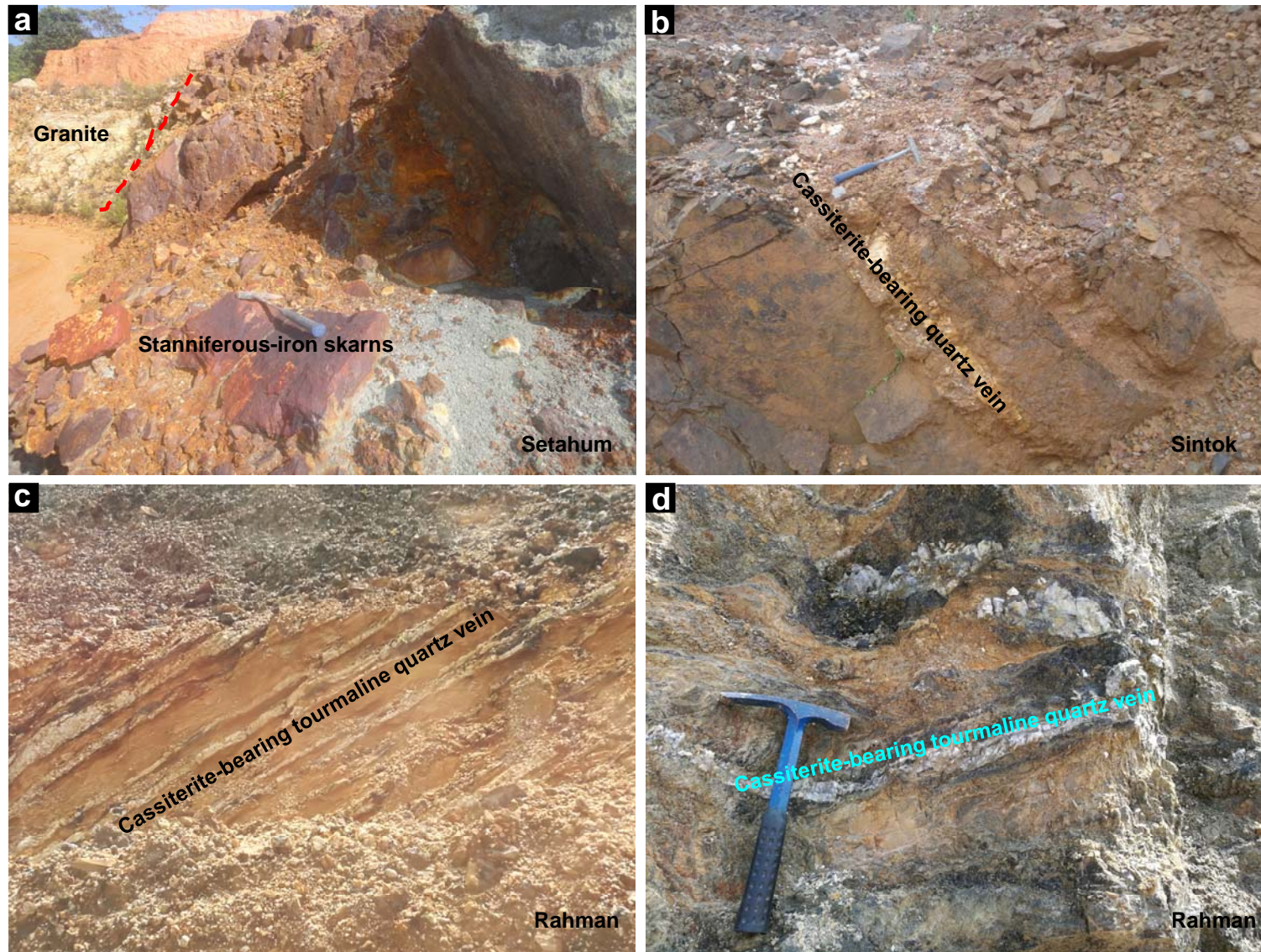


Fig. 4

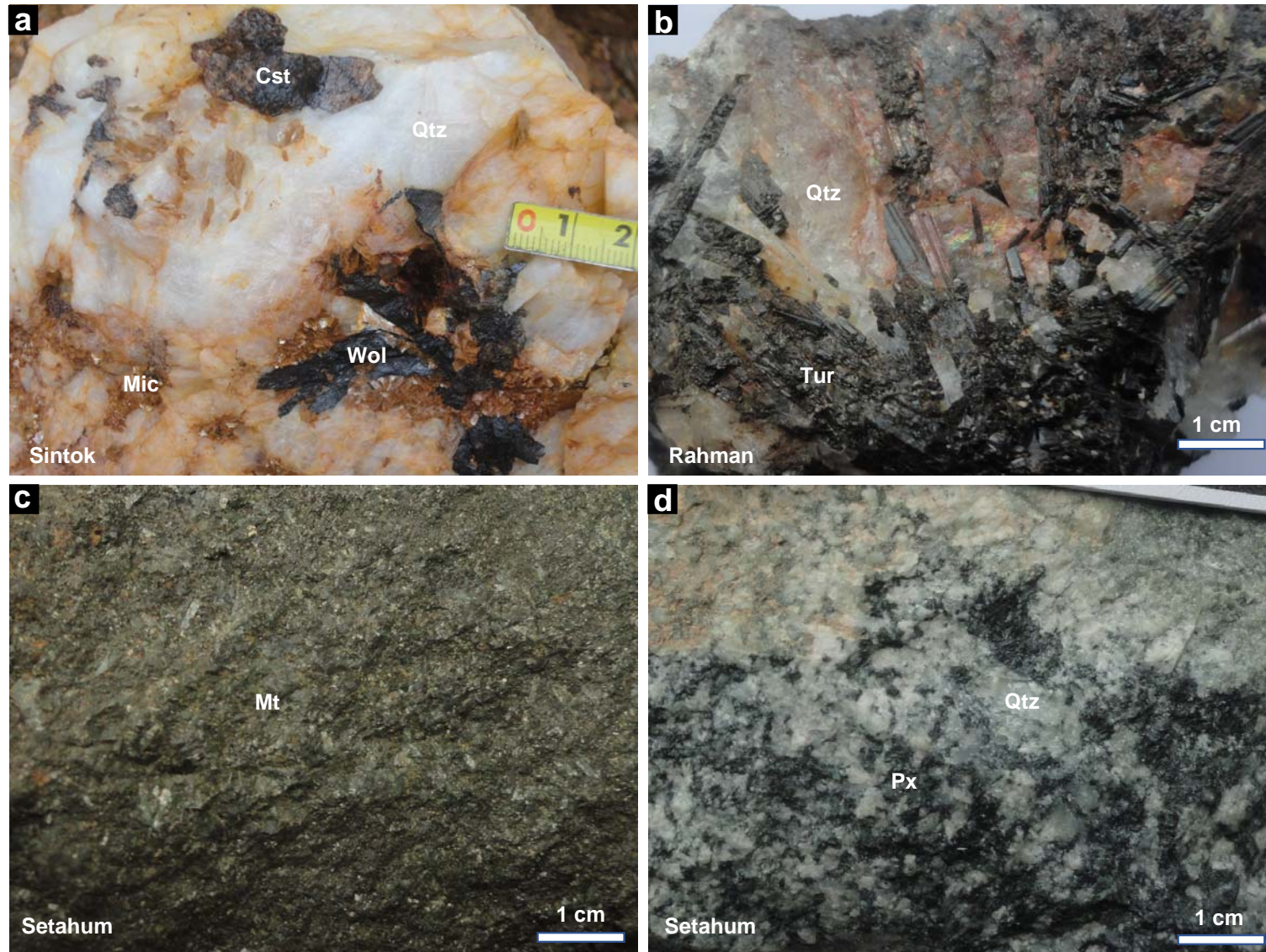
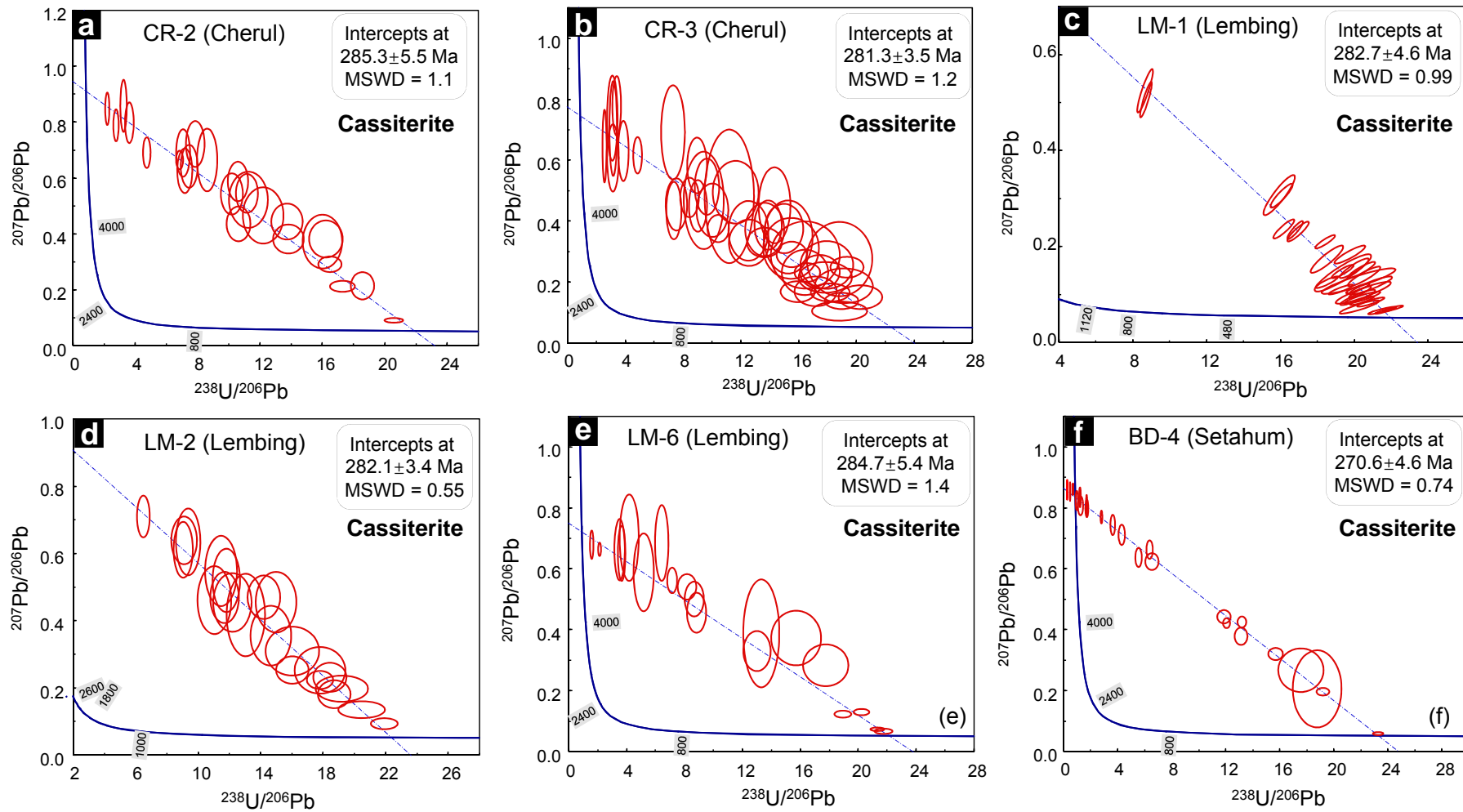


Fig. 5



Continued (Fig. 5)

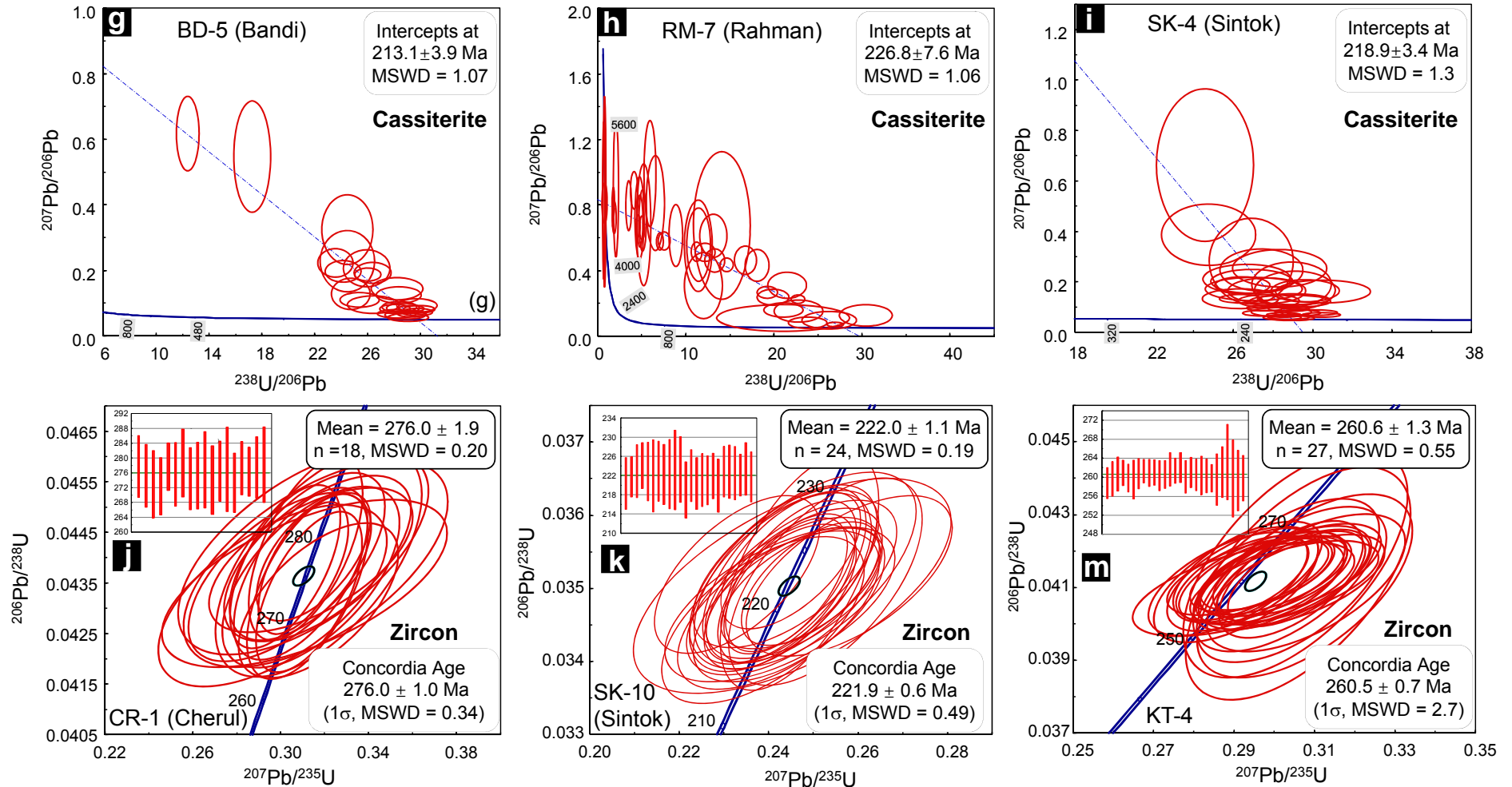


Fig. 6

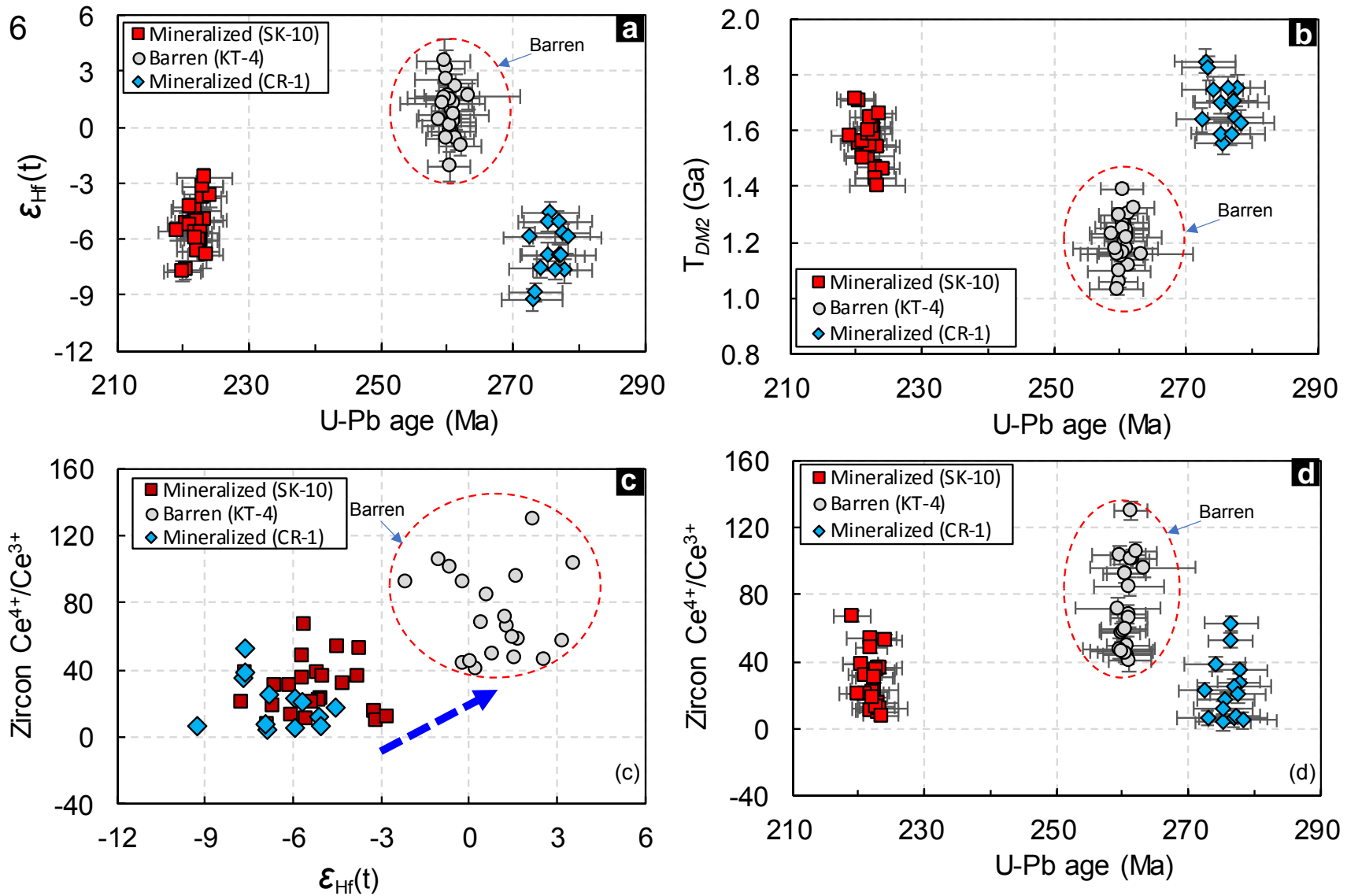


Fig. 7

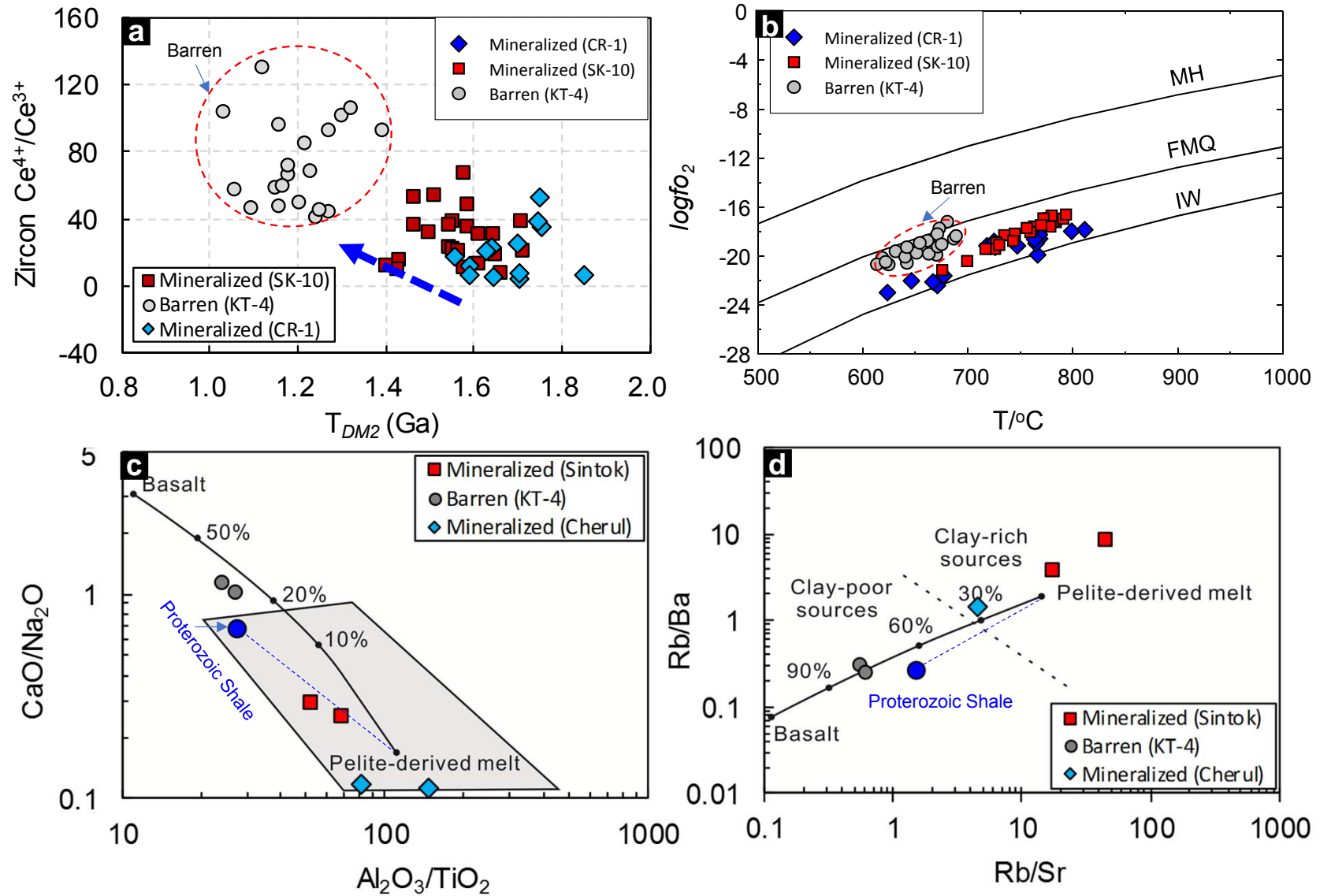


Fig. 8

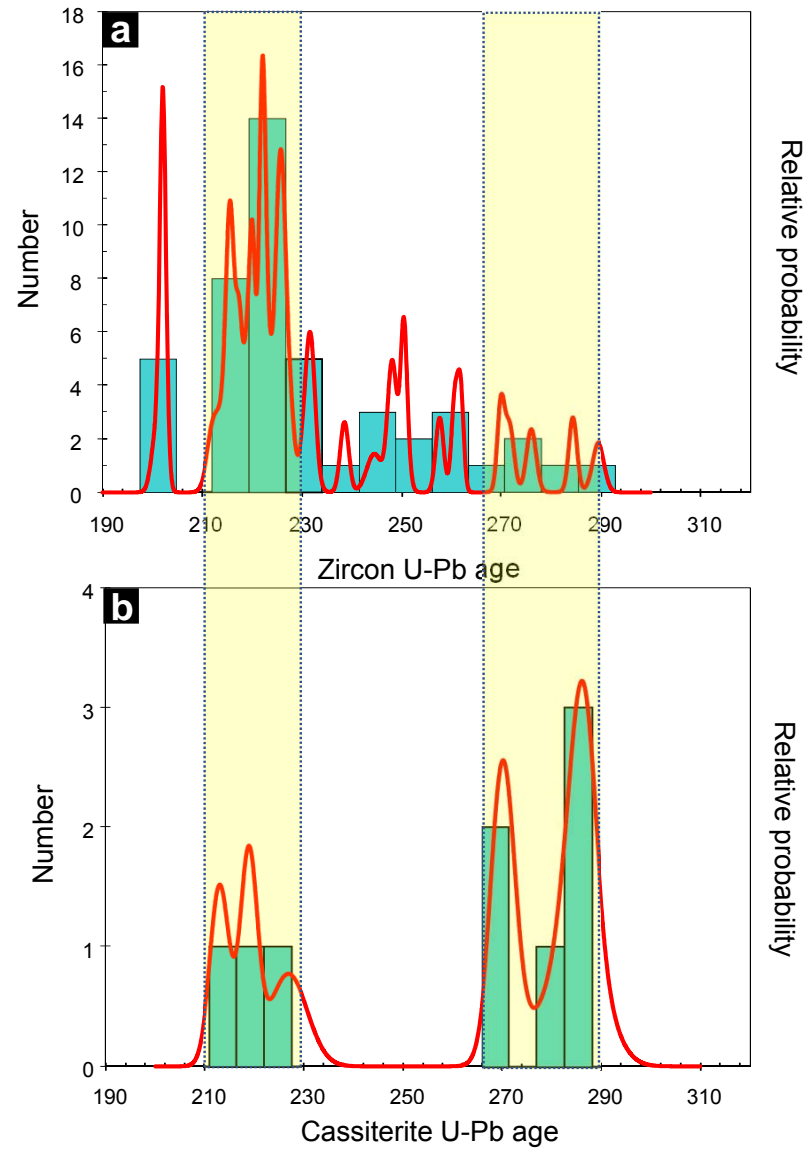


Fig. 9

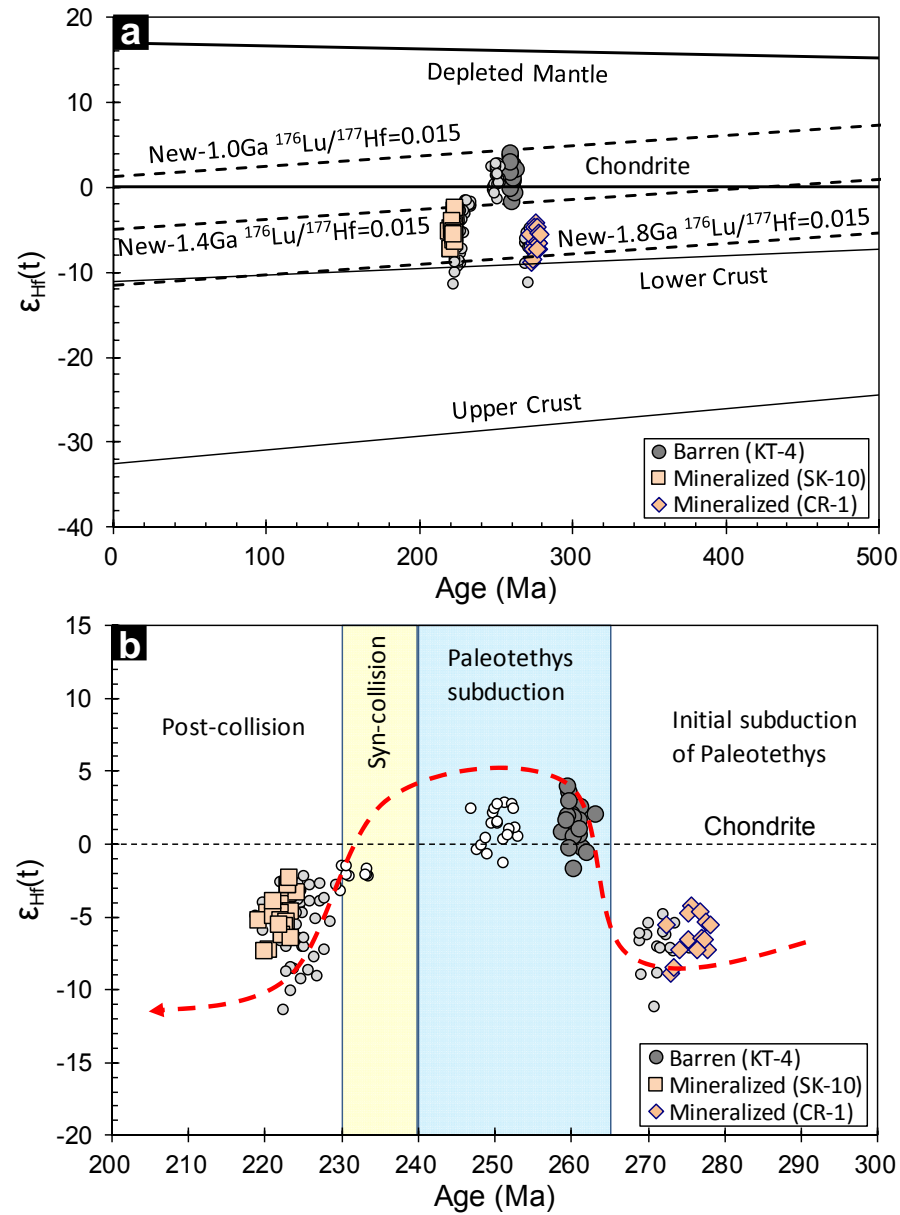


Fig. 10

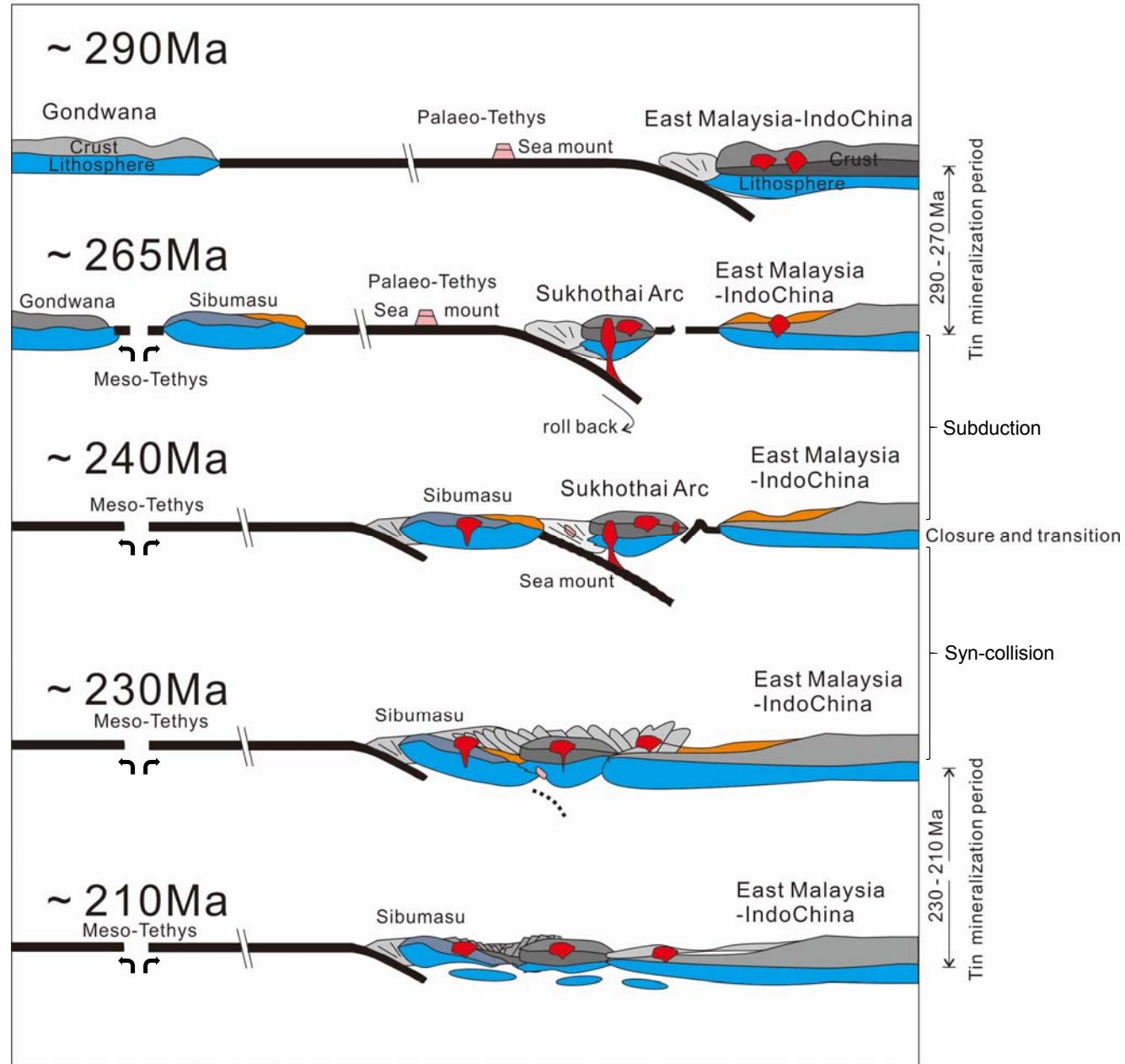


Table 1 Sample location and U-Pb ages of cassiterite and zircon

Samples	Sample location	Deposit name	Mineralization type	Cassiterite U-Pb age	Zircon U-Pb age
SK-4/SK-10	6°24'36.837"N 100°32'2.581"E	Sintok	Vein type	218.9±3.4Ma	220.0±1.1Ma
RM-7	5°38'32.113"N 101°2'6.442"E	Rahman	Vein type	226.8±7.6 Ma	
BD-5	4°18'14.624"N 103°7'44.339"E	Bandi	Vein type	213.1±3.9 Ma	
BD-4	4°17'33.974"N 103°11'12.652"E	Setahum	Stanniferous-iron skarns	270.6±4.6 Ma	
CR-1/CR-2/CR-3	4°10'26.897"N 103°10'48.669"E	Cherul	Stanniferous-iron skarns	285.3±5.5Ma 281.3±3.5Ma	276.0±1.9Ma
LM-1/LM-2	3°53'0.044"N 103°3'21.191"E	Lembing (southern)	Vein-type	282.7±4.6 Ma 282.1±3.4 Ma	
LM-6	3°54'38.673"N 103°3'11.27"E	Lembing (northern)	Vein-type	284.7±5.4 Ma	
KT-4	3°52'29.517"N 103°20'18.305"E				260.6±1.3Ma

Table 2 Zircon U-Pb and Lu-Hf isotopes of both tin-bearing and barren granites

Sample	Th	U	Th/U	²⁰⁷ Pb/ ²⁰⁶ Pb	²⁰⁷ Pb/ ²³⁵ U	²⁰⁶ Pb/ ²³⁸ U	²⁰⁸ Pb/ ²³² Th	²³⁸ U/ ²³² Th	²⁰⁷ Pb/ ²⁰⁶ Pb	²⁰⁷ Pb/ ²³⁵ U	²⁰⁶ Pb/ ²³⁸ U	¹⁷⁶ Hf/ ¹⁷⁷ Hf	¹⁷⁶ Lu/ ¹⁷⁷ Hf				
Spot	ppm	ppm	Ratio	Ratio	Ratio	2σ	Ratio	2σ	Ratio	Ratio	Age (Ma)	Age (Ma)	Age (Ma)	σ	Ratio	2σ	Ratio
CR-1 from Cherul tin deposit																	
CR-1-1	227	543	0.42	0.0516	0.3122	0.0145	0.0440	0.0007	0.0142	2.4442	333	276	278	4	0.282398	0.000018	0.000951
CR-1-3	164	281	0.58	0.0496	0.2996	0.0170	0.0436	0.0007	0.0141	1.7553	176	266	275	4	0.282424	0.000020	0.001311
CR-1-4	82.4	274	0.30	0.0498	0.2962	0.0212	0.0432	0.0007	0.0134	3.3562	187	263	273	5	0.282360	0.000017	0.001634
CR-1-8	166	582	0.29	0.0529	0.3171	0.0148	0.0432	0.0006	0.0147	3.5373	324	280	272	4	0.282454	0.000014	0.001477
CR-1-9	261	609	0.43	0.0517	0.3149	0.0106	0.0440	0.0005	0.0138	2.3794	333	278	278	3	0.282566	0.000020	0.000926
CR-1-10	515	2446	0.21	0.0508	0.3092	0.0125	0.0437	0.0007	0.0135	4.7861	232	274	276	4	0.282486	0.000017	0.000763
CR-1-14	129	288	0.45	0.0517	0.3138	0.0165	0.0436	0.0007	0.0130	2.2693	333	277	275	5	0.282474	0.000015	0.001328
CR-1-15	105	193	0.54	0.0517	0.3159	0.0246	0.0439	0.0008	0.0143	1.8699	272	279	277	5	0.282473	0.000016	0.001008
CR-1-17	251	1241	0.20	0.0519	0.3122	0.0112	0.0434	0.0007	0.0158	4.9040	280	276	274	5	0.282405	0.000014	0.001576
CR-1-18	286	904	0.32	0.0498	0.3019	0.0102	0.0438	0.0007	0.0159	3.1371	183	268	276	4	0.282175	0.000013	0.000871
CR-1-19	212	461	0.46	0.0518	0.3173	0.0192	0.0439	0.0009	0.0160	2.1710	280	280	277	6	0.282423	0.000015	0.001077
CR-1-21	299	1224	0.24	0.0519	0.3128	0.0099	0.0433	0.0006	0.0163	4.0030	280	276	273	4	0.282368	0.000014	0.001067
CR-1-24	99.1	182	0.55	0.0520	0.3138	0.0189	0.0440	0.0006	0.0171	1.7862	283	277	277	4	0.282421	0.000017	0.001028
CR-1-26	365	2059	0.18	0.0512	0.3104	0.0083	0.0438	0.0005	0.0190	5.4492	256	274	276	3	0.282403	0.000015	0.001562
CR-1-29	146	337	0.43	0.0521	0.3167	0.0174	0.0440	0.0007	0.0188	2.2389	287	279	277	4	0.282455	0.000014	0.001112
CR-1-30	244	431	0.57	0.0513	0.3103	0.0233	0.0441	0.0008	0.0194	1.6982	257	274	278	5	0.282456	0.000025	0.002651
CR-1-20	133	448	0.30	0.1093	4.8603	0.0979	0.3208	0.0034	0.1062	3.3932	1789	1795	1794	17	0.281920	0.000021	0.001190
CR-1-25	198	227	0.87	0.1031	4.5470	0.1227	0.3186	0.0054	0.1173	1.1194	1681	1740	1783	27	0.281756	0.000016	0.000894
Barren granite																	
KT-4-1	918	2624	0.35	0.0513	0.2924	0.0113	0.0410	0.0005	0.0137	2.7824	257	260	259	3	0.282645	0.000023	0.002475
KT-4-3	584	1454	0.40	0.0531	0.3026	0.0088	0.0413	0.0006	0.0125	2.4428	332	268	261	4	0.282623	0.000022	0.001541
KT-4-4	559	1695	0.33	0.0512	0.2934	0.0082	0.0413	0.0004	0.0126	2.9657	250	261	261	3	0.282642	0.000011	0.001897
KT-4-5	570	1484	0.38	0.0530	0.3025	0.0096	0.0411	0.0005	0.0130	2.5627	328	268	260	3	0.282718	0.000027	0.001481
KT-4-6	783	2184	0.36	0.0510	0.2906	0.0084	0.0411	0.0007	0.0128	2.7972	239	259	260	4	0.282734	0.000032	0.002445
KT-4-7	732	1872	0.39	0.0519	0.2969	0.0084	0.0413	0.0005	0.0131	2.5225	283	264	261	3	0.282653	0.000024	0.001878
KT-4-8	1320	3530	0.37	0.0519	0.2980	0.0067	0.0414	0.0004	0.0129	2.6472	283	265	261	2	0.282691	0.000018	0.001917
KT-4-10	991	2489	0.40	0.0523	0.2995	0.0076	0.0413	0.0004	0.0134	2.4772	298	266	261	3	0.282667	0.000021	0.002065
KT-4-11	938	2405	0.39	0.0536	0.3064	0.0086	0.0412	0.0005	0.0130	2.5921	354	271	260	3	0.282570	0.000022	0.001890
KT-4-12	1332	3484	0.38	0.0511	0.2921	0.0068	0.0412	0.0005	0.0134	2.6710	256	260	261	3	0.282624	0.000016	0.001852
KT-4-13	854	2344	0.36	0.0512	0.2933	0.0076	0.0414	0.0006	0.0140	2.8669	256	261	262	4	0.282478	0.000020	0.001872
KT-4-14	1076	2805	0.38	0.0518	0.2971	0.0073	0.0414	0.0004	0.0130	2.6141	276	264	261	3	0.282612	0.000016	0.002133
KT-4-15	807	2259	0.36	0.0532	0.3057	0.0086	0.0415	0.0005	0.0137	2.9605	339	271	262	3	0.282600	0.000015	0.001725
KT-4-16	714	2245	0.32	0.0523	0.2990	0.0078	0.0412	0.0006	0.0134	3.1890	298	266	260	3	0.282679	0.000033	0.002040
KT-4-17	682	1514	0.45	0.0532	0.3047	0.0077	0.0413	0.0005	0.0135	2.2824	339	270	261	3	0.282635	0.000019	0.001570
KT-4-19	961	2189	0.44	0.0532	0.3042	0.0073	0.0412	0.0007	0.0130	2.2791	339	270	260	4	0.282633	0.000016	0.001897
KT-4-20	996	2078	0.48	0.0511	0.2922	0.0077	0.0412	0.0006	0.0129	2.0926	256	260	260	4	0.282672	0.000018	0.002040
KT-4-21	984	2770	0.36	0.0523	0.2989	0.0075	0.0411	0.0005	0.0135	2.8836	298	266	260	3	0.282613	0.000033	0.002019
KT-4-24	483	1201	0.40	0.0535	0.3043	0.0096	0.0411	0.0009	0.0131	2.5064	350	270	260	5	0.282674	0.000023	0.001628
KT-4-25	811	2433	0.33	0.0527	0.3029	0.0095	0.0413	0.0009	0.0138	3.0295	322	269	261	5	0.282649	0.000026	0.002097
KT-4-26	1187	2960	0.40	0.0532	0.3053	0.0114	0.0417	0.0013	0.0132	2.5255	345	270	263	8	0.282676	0.000020	0.002149
KT-4-29	718	2099	0.34	0.0541	0.3075	0.0109	0.0410	0.0010	0.0138	3.1874	376	272	259	6	0.282666	0.000021	0.001890
KT-4-30	1644	3819	0.43	0.0540	0.3080	0.0101	0.0411	0.0008	0.0131	2.3882	369	273	260	5	0.282705	0.000030	0.002508

SK-10 from sintok deposit

SK-10(2)-1	199	483	0.41	0.0511	0.2446	0.0088	0.0348	0.0004	0.0102	2.4156	256	222	220	3	0.282505	0.000016	0.001127
SK-10(2)-4	442	862	0.51	0.0510	0.2472	0.0073	0.0350	0.0003	0.0105	1.9144	243	224	222	2	0.282495	0.000015	0.001511
SK-10(2)-6	329	1209	0.27	0.0479	0.2330	0.0075	0.0352	0.0004	0.0113	3.5709	94.5	213	223	3	0.282544	0.000016	0.001493
SK-10(2)-7	295	1250	0.24	0.0497	0.2449	0.0064	0.0354	0.0004	0.0109	4.1316	189	222	224	2	0.282546	0.000015	0.001889
SK-10(2)-8	284	857	0.33	0.0502	0.2435	0.0075	0.0352	0.0005	0.0114	3.0705	211	221	223	3	0.282563	0.000015	0.002152
SK-10(2)-10	169	758	0.22	0.0506	0.2453	0.0145	0.0350	0.0006	0.0117	4.4042	233	223	222	4	0.282523	0.000015	0.000990
SK-10(2)-11	359	661	0.54	0.0501	0.2438	0.0084	0.0352	0.0005	0.0113	1.8320	211	222	223	3	0.282561	0.000017	0.001324
SK-10(2)-12	226	739	0.31	0.0499	0.2427	0.0083	0.0351	0.0005	0.0109	3.2601	191	221	222	3	0.282465	0.000016	0.001905
SK-10(2)-13	235	692	0.34	0.0523	0.2527	0.0088	0.0351	0.0006	0.0116	2.8441	302	229	222	4	0.282508	0.000014	0.001284
SK-10(2)-14	1425	3061	0.47	0.0505	0.2470	0.0072	0.0352	0.0007	0.0113	2.0884	217	224	223	4	0.282573	0.000014	0.001573
SK-10(2)-15	497	991	0.50	0.0509	0.2477	0.0104	0.0352	0.0005	0.0111	2.1401	235	225	223	3	0.282508	0.000016	0.001001
SK-10(2)-16	336	1550	0.22	0.0498	0.2388	0.0093	0.0346	0.0005	0.0120	4.5211	187	217	219	3	0.282494	0.000014	0.001345
SK-10(2)-17	288	807	0.36	0.0509	0.2458	0.0080	0.0350	0.0004	0.0106	2.7384	235	223	222	3	0.282506	0.000015	0.001417
SK-10(2)-18	301	888	0.34	0.0504	0.2425	0.0105	0.0348	0.0004	0.0109	2.9355	217	220	220	3	0.282434	0.000014	0.001023
SK-10(2)-19	370	845	0.44	0.0505	0.2436	0.0089	0.0349	0.0004	0.0111	2.2500	220	221	221	3	0.282500	0.000016	0.001234
SK-10(2)-21	340	831	0.41	0.0504	0.2426	0.0070	0.0349	0.0004	0.0107	2.4773	213	221	221	3	0.282530	0.000021	0.001409
SK-10(2)-22	514	3055	0.17	0.0503	0.2438	0.0056	0.0350	0.0004	0.0112	5.8206	209	222	222	2	0.282492	0.000014	0.001725
SK-10(2)-23	255	696	0.37	0.0503	0.2422	0.0092	0.0347	0.0004	0.0104	2.6945	209	220	220	3	0.282433	0.000015	0.001196
SK-10(2)-24	704	1297	0.54	0.0505	0.2451	0.0060	0.0352	0.0004	0.0116	1.8518	217	223	223	3	0.282481	0.000015	0.001674
SK-10(2)-25	248	1776	0.14	0.0530	0.2580	0.0094	0.0352	0.0004	0.0111	7.0237	332	233	223	3	0.282491	0.000014	0.001610
SK-10(2)-27	248	577	0.43	0.0509	0.2473	0.0088	0.0351	0.0004	0.0106	2.3042	235	224	223	3	0.282480	0.000017	0.001768
SK-10(2)-28	508	4870	0.10	0.0512	0.2494	0.0063	0.0351	0.0003	0.0110	9.6079	250	226	222	2	0.282469	0.000013	0.003088
SK-10(2)-29	244	580	0.42	0.0503	0.2439	0.0085	0.0353	0.0004	0.0114	2.4457	209	222	223	3	0.282456	0.000019	0.001339
SK-10(2)-30	190	2752	0.07	0.0504	0.2440	0.0063	0.0350	0.0004	0.0111	13.9617	213	222	222	3	0.282484	0.000014	0.001745

$^{176}\text{Yb}/^{177}\text{Hf}$	$\epsilon_{\text{Hf}}(t)$		T_{DM}	T_{DM2}
Ratio	ϵ	2σ	Ga	Ga
0.039311	-7.7	0.6	1.2	1.8
0.045409	-6.9	0.7	1.2	1.7
0.055398	-9.3	0.6	1.3	1.8
0.054295	-5.9	0.5	1.1	1.6
0.032816	-1.7	0.7	1.0	1.4
0.027190	-4.6	0.6	1.1	1.6
0.060587	-5.1	0.5	1.1	1.6
0.045759	-5.1	0.6	1.1	1.6
0.072011	-7.6	0.5	1.2	1.7
0.038979	-15.6	0.5	1.5	2.2
0.045258	-6.8	0.5	1.2	1.7
0.047427	-8.9	0.5	1.3	1.8
0.044780	-6.9	0.6	1.2	1.7
0.070520	-7.7	0.5	1.2	1.8
0.048287	-5.7	0.5	1.1	1.6
0.106470	-5.9	0.9	1.2	1.6
0.049617	8.5	0.7	1.9	1.9
0.039602	2.8	0.6	2.1	2.3
0.105306	0.4	0.8	0.9	1.2
0.064990	-0.2	0.8	0.9	1.3
0.077754	0.4	0.4	0.9	1.2
0.063083	3.2	1.0	0.8	1.1
0.095813	3.6	1.1	0.8	1.0
0.081125	0.8	0.8	0.9	1.2
0.077023	2.2	0.6	0.8	1.1
0.089322	1.3	0.7	0.9	1.2
0.077964	-2.1	0.8	1.0	1.4
0.082210	-0.2	0.6	0.9	1.3
0.082967	-5.4	0.7	1.1	1.6
0.091276	-0.7	0.6	0.9	1.3
0.073260	-1.0	0.5	0.9	1.3
0.082414	1.7	1.2	0.8	1.2
0.071618	0.2	0.7	0.9	1.2
0.078268	0.1	0.6	0.9	1.3
0.087610	1.5	0.6	0.8	1.2
0.079598	-0.6	1.2	0.9	1.3
0.065387	1.6	0.8	0.8	1.2
0.089659	0.6	0.9	0.9	1.2
0.083736	1.6	0.7	0.8	1.2
0.080920	1.2	0.7	0.8	1.2
0.097934	2.5	1.1	0.8	1.1

0.046851	-5.2	0.6	1.1	1.6
0.065717	-5.5	0.5	1.1	1.6
0.063016	-3.8	0.6	1.0	1.5
0.073666	-3.7	0.5	1.0	1.5
0.086826	-3.2	0.5	1.0	1.4
0.041608	-4.5	0.5	1.0	1.5
0.056231	-3.2	0.6	1.0	1.4
0.083971	-6.7	0.6	1.1	1.6
0.048851	-5.0	0.5	1.1	1.5
0.069686	-2.8	0.5	1.0	1.4
0.042018	-5.0	0.6	1.1	1.5
0.059169	-5.6	0.5	1.1	1.6
0.059752	-5.1	0.5	1.1	1.6
0.044598	-7.7	0.5	1.2	1.7
0.051669	-5.3	0.6	1.1	1.6
0.057555	-4.3	0.7	1.0	1.5
0.073193	-5.7	0.5	1.1	1.6
0.050870	-7.8	0.5	1.2	1.7
0.074791	-6.1	0.5	1.1	1.6
0.068109	-5.7	0.5	1.1	1.6
0.068912	-6.1	0.6	1.1	1.6
0.131832	-6.7	0.5	1.2	1.6
0.059035	-6.9	0.7	1.1	1.7
0.073911	-6.0	0.5	1.1	1.6

Table 3 Zircon trace element and calculated parameters

Spot no.	Age (Ma)	$\pm\sigma$	Li	Al	P	Ti	Cr	Rb	Sr	Y	Nb	Sn	La	Ce	Pr	Nd
CR-1 from Cherul tin deposit																
CR-1-1	278	4	1.75	1.41	369	5.08	2.05	0.12	1.32	1025	3.53	0.07	0.009	4.79	0.058	1.35
CR-1-3	275	4	3.44	0.80	291	7.98	-	0.29	0.49	1692	1.25	0.54	0.015	3.02	0.237	4.47
CR-1-4	273	5	3.41	27.5	830	7.82	2.23	0.30	2.79	1415	1.20	0.21	0.054	1.43	0.063	1.53
CR-1-8	272	4	2.13	127	958	6.38	0.48	0.77	4.89	2179	3.60	0.13	0.623	3.81	0.209	2.01
CR-1-9	278	3	2.24	1.16	318	4.65	1.80	0.17	2.01	1275	3.87	0.12	0.006	5.85	0.067	1.74
CR-1-10	276	4	16.0	4.24	617	2.66	2.07	0.25	-	1348	7.06	0.07	0.009	4.16	0.072	1.15
CR-1-14	275	5	0.65	1.28	513	7.69	1.31	0.21	3.41	1522	1.17	0.32	0.000	2.54	0.085	1.99
CR-1-15	277	5	1.14	12.6	600	12.1	1.73	0.22	4.29	1334	1.07	0.24	0.018	2.34	0.137	2.61
CR-1-17	274	5	2.91	3.40	1158	2.53	1.52	0.53	6.17	3093	6.27	0.23	0.002	3.27	0.044	1.06
CR-1-18	276	4	2.01	2.44	374	1.94	1.53	0.31	3.38	1231	3.84	0.28	0.006	3.90	0.031	0.81
CR-1-19	277	6	0.45	1.38	278	5.02	1.44	0.14	0.053	1182	3.05	0.16	0.250	5.75	0.133	1.99
CR-1-21	273	4	2.71	0.68	270	1.43	0.89	0.20	2.30	1136	4.61	0.06	0.003	3.58	0.015	0.65
CR-1-24	277	4	0.40	2.27	535	10.8	0.021	0.18	3.56	1280	1.01	-	0.000	2.39	0.112	2.04
CR-1-26	276	3	7.77	30.0	1243	2.88	1.80	0.72	2.33	2867	7.07	0.21	0.025	4.58	0.082	1.26
CR-1-29	277	4	0.89	2.55	376	7.95	0.86	0.23	0.77	1171	2.16	0.06	0.006	3.79	0.077	1.81
CR-1-30	278	5	0.095	0.26	255	7.58	1.74	0.21	3.01	1526	0.97	0.13	0.011	3.34	0.294	4.46
CR-1-20	1794	17	0.50	6.98	299	6.20	3.13	0.16	1.34	1036	3.34	0.17	0.010	5.79	0.082	1.55
CR-1-25	1783	27	0.066	1.84	510	12.6	2.73	0.20	1.95	1576	1.17	0.50	0.008	14.5	0.164	2.78
Barren granite																
KT-4-1	259	3	54.9	65.8	2277	3.00	0.71	0.78	6.06	4039	24.3	0.32	10.51	52.1	6.855	41.9
KT-4-3	261	4	10.6	5.30	500	3.23	0.90	0.51	3.46	2492	10.7	0.11	0.063	8.27	0.086	2.20
KT-4-4	261	3	13.4	0.29	610	1.82	3.41	0.46	2.08	2656	11.5	0.09	0.003	7.73	0.059	1.50
KT-4-5	260	3	9.07	0.46	549	2.64	1.72	0.48	3.98	2851	14.0	0.08	0.004	9.64	0.052	1.97
KT-4-6	260	4	13.4	1.74	742	2.41	2.09	0.45	4.28	3068	19.8	0.19	0.009	10.6	0.062	1.42
KT-4-7	261	3	12.9	0.12	616	1.34	2.37	0.42	7.32	2920	12.9	0.06	0.003	9.59	0.101	2.35
KT-4-8	261	2	15.8	4.07	627	1.84	2.76	0.65	4.51	3841	35.7	0.03	0.084	16.1	0.094	1.73
KT-4-10	261	3	18.0	-	593	1.43	0.89	0.60	5.09	3591	28.7	0.06	0.331	17.3	0.234	3.23
KT-4-11	260	3	27.9	66.1	693	2.67	1.56	1.00	4.97	2801	20.6	0.24	0.017	8.51	0.043	1.31
KT-4-12	261	3	30.4	0.27	897	1.60	1.04	19.7	7.12	4212	26.2	0.42	0.012	11.9	0.066	1.66
KT-4-13	262	4	16.4	0.63	795	1.80	1.92	0.39	1.91	2767	17.0	0.27	0.000	8.49	0.051	1.26
KT-4-14	261	3	22.0	0.19	816	1.25	1.65	0.54	5.56	3369	20.9	0.16	0.036	10.9	0.075	1.48
KT-4-15	262	3	12.1	0.83	852	2.08	2.25	0.44	6.51	2907	14.5	0.34	0.000	7.85	0.041	1.08
KT-4-16	260	3	21.2	0.34	821	0.88	2.84	0.53	3.33	3234	11.5	0.15	0.006	6.90	0.037	1.66
KT-4-17	261	3	13.5	11.7	718	1.84	1.41	0.54	3.46	2799	10.9	0.15	0.076	8.82	0.159	2.61
KT-4-19	260	4	17.9	0.90	649	3.31	2.51	0.57	3.30	3785	19.9	0.17	0.223	14.3	0.275	3.59
KT-4-20	260	4	12.5	3.69	540	2.73	1.68	0.72	4.97	3288	21.1	0.31	0.157	13.3	0.170	2.58
KT-4-21	260	3	27.7	60.0	2275	2.67	2.90	0.80	7.62	3564	19.3	0.37	6.109	34.3	4.013	25.2
KT-4-24	260	5	10.7	0.17	499	1.46	0.49	0.43	3.24	2485	10.9	0.26	0.007	7.32	0.066	1.82
KT-4-25	261	5	24.5	0.64	1002	2.37	2.55	0.51	4.72	3032	11.8	0.21	0.000	6.99	0.048	1.15
KT-4-26	263	8	16.3	0.88	742	2.81	1.94	0.56	4.92	3168	23.4	0.18	0.006	11.4	0.041	1.76
KT-4-29	259	6	37.1	1.48	667	1.40	1.24	0.56	4.46	3200	13.8	0.81	0.042	7.80	0.066	1.54
KT-4-30	260	5	30.0	-	915	2.16	0.23	0.58	5.79	3790	31.2	0.48	1.181	19.0	0.757	5.82
SK-10 from sintok deposit																
SK-10-1	220	3	7.40	1.69	677	8.71	2.01	0.24	1.78	1389	2.39	2.49	0.011	6.05	0.072	1.21
SK-10-4	222	2	11.8	-	1215	9.49	0.93	0.32	2.06	1969	3.31	2.68	6.925	27.8	2.369	14.2
SK-10-6	223	3	16.8	1.22	1066	7.56	1.63	0.38	3.24	2214	3.81	2.50	0.002	7.36	0.052	1.58
SK-10-7	224	2	15.8	7.27	1002	5.58	0.52	0.40	2.45	2225	4.88	2.53	0.088	7.08	0.078	1.18
SK-10-8	223	3	8.76	11.2	953	6.23	2.10	0.42	6.37	2340	2.62	2.52	0.065	5.76	0.186	2.51
SK-10-10	222	4	10.9	2.94	691	5.14	1.19	0.21	5.43	1334	3.23	2.49	0.005	4.14	0.041	0.63
SK-10-11	223	3	8.94	4.46	666	9.31	1.48	0.26	1.79	1720	2.72	2.47	0.007	5.74	0.167	2.83
SK-10-12	222	3	12.3	104	651	5.08	2.49	0.57	2.04	1521	5.50	2.86	0.024	6.64	0.120	1.63
SK-10-13	222	4	8.93	13.1	666	7.29	2.24	0.27	2.20	1411	3.92	0.00	1.708	11.6	0.640	3.81
SK-10-14	223	4	25.0	43.7	1237	8.25	1.14	2.07	3.72	2383	18.3	3.26	19.499	78.0	6.680	32.3
SK-10-15	223	3	8.33	6.18	650	6.13	1.17	0.46	2.60	1982	3.73	2.85	0.039	14.2	0.175	2.48
SK-10-16	219	3	19.1	1.35	881	4.59	1.40	0.35	-	1913	6.09	2.24	0.000	7.59	0.054	1.06
SK-10-17	222	3	13.6	3.90	1096	9.12	1.55	0.35	5.05	2127	2.88	2.15	0.010	6.21	0.072	1.91
SK-10-18	220	3	12.6	1.66	935	7.02	1.99	0.36	2.77	1888	3.33	2.11	0.002	7.93	0.078	1.51
SK-10-19	221	3	9.36	1.07	892	8.94	1.66	0.33	4.19	1782	3.18	2.13	0.501	8.87	0.252	2.74
SK-10-21	221	3	12.0	1.14	762	8.27	0.95	0.35	1.94	1737	3.26	2.08	0.020	8.44	0.098	1.73
SK-10-22	222	2	27.0	0.39	1589	3.75	3.75	0.52	6.14	3482	10.1	2.53	0.003	8.55	0.062	1.59
SK-10-23	220	3	9.46	10.6	957	9.97	1.24	0.34	4.41	1937	2.65	2.09	0.002	5.99	0.096	1.91
SK-10-24	223	3	13.7	30.7	1162	8.83	2.35	0.60	2.04	2221	6.09	2.32	3.897	20.3	1.665	9.72
SK-10-25	223	3	28.9	8.71	1002	5.30	1.55	0.35	4.54	2000	5.91	2.43	0.061	5.20	0.080	1.48
SK-10-27	223	3	8.50	1.36	664	8.09	1.77	0.30	2.66	1424	2.83	2.17	0.003	7.67	0.045	1.76
SK-10-28	222	2	54.0	21.0	2058	2.82	3.00	0.74	7.13	4609	19.2	2.71	0.284	8.80	0.572	4.38
SK-10-29	223	3	10.4	38.9	1968	10.2	1.34	0.81	6.45	3784	1.77	2.23	3.097	13.0	1.403	9.84
SK-10-30	222	3	30.4	0.93	1225	0.63	4.27	0.49	5.58	2616	6.06	2.39	0.004	3.06	0.014	0.36

Sm	Eu	Gd	Tb	Dy	Ho	Er	Tm	Yb	Lu	Hf	Ta	Th	U	δCe	δEu	$\text{Ce}^{4+}/\text{Ce}^{3+}$
3.14	0.129	20.6	7.24	88.6	35.1	162	33.0	292	60.4	12787	2.03	227	543	52.6	0.05	34.6
7.99	0.595	45.2	14.3	163	59.3	245	47.3	416	80.1	10433	0.69	164	281	12.4	0.10	3.7
4.01	0.257	28.6	10.9	129	45.1	188	35.7	311	60.1	12969	0.68	82.4	274	6.0	0.07	6.6
5.17	0.228	35.1	13.6	175	72.5	344	72.5	666	137	13156	1.74	166	582	2.6	0.05	22.4
4.79	0.211	26.8	9.40	113	43.5	193	39.7	351	70.4	12164	2.20	261	609	74.7	0.06	27.8
5.97	0.508	44.7	15.1	147	44.0	170	31.4	276	52.2	15730	3.67	515	2446	39.0	0.10	16.9
4.30	0.236	29.8	11.0	130	51.4	233	47.1	409	81.5	12570	0.74	129	288	-	0.06	11.7
5.49	0.305	32.3	10.9	125	45.7	202	39.8	348	69.2	11280	0.65	105	193	11.6	0.07	6.0
5.30	0.165	45.1	19.3	260	105	478	98.4	886	178	16918	4.01	251	1241	88.2	0.03	38.5
2.40	0.108	19.3	7.80	102	41.1	196	41.2	382	77.7	13679	3.12	286	904	67.8	0.05	62.9
4.02	0.236	26.9	8.75	107	39.9	180	36.5	316	65.4	11667	1.66	212	461	7.7	0.07	25.0
1.75	0.160	15.5	6.30	86.9	36.1	178	39.5	377	80.7	13748	3.76	299	1224	132.9	0.09	-
5.91	0.229	32.2	10.5	122	44.7	194	38.2	334	66.9	11195	0.58	99.1	182	-	0.05	7.4
4.43	0.192	39.8	17.1	234	95.7	449	95.8	874	176	15936	5.65	365	2059	24.7	0.04	52.4
3.52	0.246	24.0	8.48	103	39.0	179	37.0	333	68.4	11319	1.08	146	337	42.6	0.08	20.3
8.14	1.618	38.9	11.5	130	49.3	228	47.9	459	99.6	8514	0.46	244	431	14.4	0.28	5.0
4.22	0.328	23.0	8.01	92.6	35.1	156	32.2	293	61.2	11529	1.50	133	448	50.0	0.10	-
6.54	0.765	40.3	13.3	151	56.4	240	45.9	398	78.9	11656	0.81	198	227	97.4	0.14	-
24.8	0.412	86.9	29.9	361	134	580	114	966	185	15284	7.23	918	2624	1.5	0.03	-
7.13	0.350	46.2	17.4	216	84.5	371	73.5	634	125	13942	4.00	584	1454	27.6	0.06	43.9
5.84	0.214	47.3	17.8	229	89.7	401	78.9	686	134	14930	4.76	559	1695	143.4	0.04	67.9
7.31	0.187	54.3	20.2	250	96.5	421	81.7	697	136	14849	4.93	570	1484	156.2	0.03	57.0
5.89	0.151	53.5	20.6	268	105	463	90.8	783	152	15299	7.45	783	2184	110.9	0.03	103.6
7.48	0.375	53.0	20.3	254	98.2	429	84.4	736	143	13772	4.83	732	1872	145.9	0.06	49.7
7.35	0.107	62.6	25.4	333	131	573	113	972	186	16039	14.1	1320	3530	44.3	0.02	129.6
8.74	0.190	67.2	25.3	322	122	529	103	878	168	15049	10.2	991	2489	15.3	0.02	66.2
5.27	0.110	44.8	18.5	243	92.9	416	81.8	712	137	15533	7.28	938	2405	76.5	0.02	92.0
8.77	0.159	71.1	28.4	365	142	628	123	1057	204	15836	9.15	1332	3484	101.8	0.02	92.4
4.97	0.166	42.9	17.6	234	92.3	417	82.7	723	142	14605	6.09	854	2344	431.3	0.03	101.3
6.75	0.193	55.4	22.2	289	112	502	99.2	856	167	14834	7.54	1076	2805	51.6	0.03	100.8
5.21	0.124	46.5	18.2	242	96.1	431	86.5	752	147	14611	5.47	807	2259	-	0.02	105.3
6.37	0.171	53.3	21.6	281	108	484	96.3	835	163	15180	4.60	714	2245	113.9	0.03	58.2
7.57	0.243	53.4	19.7	247	94.1	419	81.2	700	137	14152	3.93	682	1514	19.7	0.04	40.0
10.5	0.218	74.7	28.3	344	131	563	108	928	180	14865	6.92	961	2189	14.2	0.02	45.4
8.42	0.214	62.6	23.0	289	109	476	92.5	784	150	14703	7.12	996	2078	19.9	0.03	59.4
15.0	0.215	68.3	24.9	309	119	530	104	897	174	15026	6.75	984	2770	1.7	0.02	-
6.31	0.189	47.3	17.2	218	83.4	363	70.7	613	120	15170	4.21	483	1201	82.9	0.03	47.7
6.17	0.163	49.2	19.9	266	103	469	92.4	815	159	14822	4.58	811	2433	-	0.03	84.5
5.84	0.204	51.5	20.6	273	108	485	94.4	824	158	15478	9.11	1187	2960	174.9	0.04	96.0
5.95	0.208	51.0	19.7	253	98.9	449	90.7	797	158	14244	5.02	718	2099	36.5	0.04	71.9
8.61	0.190	68.7	27.1	350	134	587	113	981	186	15514	10.9	1644	3819	4.9	0.02	46.3
3.28	0.104	21.8	8.69	114	44.7	210	44.9	410	82.5	12679	1.78	199	483	53.1	0.04	38.1
8.56	0.178	39.2	14.0	168	63.2	282	57.8	511	100	12200	2.19	442	862	1.7	0.03	11.0
5.00	0.092	32.8	13.8	182	72.1	336	71.6	649	129	13685	2.73	329	1209	166.2	0.02	35.7
3.86	0.078	31.2	13.3	176	70.8	336	71.9	651	129	14204	4.15	295	1250	21.0	0.02	52.2
6.28	0.145	39.5	15.3	194	75.4	344	71.0	634	124	13124	2.12	284	857	12.9	0.03	14.7
3.07	0.029	18.0	7.94	108	44.0	218	46.8	426	86.7	13476	2.14	169	758	69.9	0.01	53.5
6.49	0.148	34.8	12.6	149	56.1	248	51.0	451	87.4	12225	1.60	359	661	42.2	0.03	10.2
3.95	0.164	23.5	9.66	124	49.0	234	50.4	468	93.3	13694	2.41	226	739	30.6	0.05	30.9
4.04	0.127	23.3	8.83	116	45.6	214	45.7	412	82.9	12652	2.48	235	692	2.7	0.04	23.1
14.9	0.532	52.4	17.8	211	78.7	349	72.0	644	125	12706	8.57	1425	3061	1.7	0.06	12.0
5.70	0.191	35.3	13.4	172	64.7	291	59.4	533	103	13155	2.57	497	991	42.2	0.04	36.3
3.36	0.080	25.8	11.1	150	62.0	300	64.6	593	120	14312	4.47	336	1550	-	0.03	66.8
5.91	0.136	35.5	14.0	176	69.9	318	66.3	603	120	12340	2.08	288	807	56.0	0.03	21.3
4.25	0.120	31.8	12.1	155	61.2	283	59.2	536	106	13205	2.44	301	888	148.3	0.03	38.5
5.23	0.093	30.8	11.6	149	57.6	261	54.5	494	95.9	12627	2.15	370	845	6.1	0.02	21.1
4.60	0.118	30.8	11.4	143	56.0	255	52.2	473	93.6	12955	2.33	340	831	46.5	0.03	32.1
5.99	0.047	44.1	20.3	277	113	535	113	1028	202	15353	7.81	514	3055	151.0	0.01	48.0
5.02	0.141	33.9	12.6	161	63.2	285	59.4	539	107	12843	1.74	255	696	104.8	0.03	20.9
8.27	0.167	42.6	15.0	185	71.3	322	66.5	596	116	12556	2.76	704	1297	2.0	0.03	12.5
3.61	0.076	24.7	11.3	155	64.0	315	69.2	660	130	14499	5.46	248	1776	18.2	0.02	34.7
3.66	0.085	24.3	9.54	121	46.9	211	43.4	389	76.9	12697	1.84	248	577	172.2	0.03	30.1
9.65	0.723	54.8	26.8	355	146	718	159	1499	299	16056	11.8	508	4870	5.4	0.10	18.5
11.6	0.221	66.2	25.4	317	122	546	111	993	190	12096	1.15	244	580	1.5	0.02	8.0
2.05	0.015	20.6	11.6	185	81.3	430	100	976	197	18041	6.80	190	2752	105.2	0.01	137.7

$T/^{\circ}C$	Th/U	Sm/Yb
726	0.42	0.011
769	0.58	0.019
767	0.30	0.013
747	0.29	0.008
718	0.43	0.014
671	0.21	0.022
765	0.45	0.011
811	0.54	0.016
667	0.20	0.006
646	0.32	0.006
725	0.46	0.013
623	0.24	0.005
799	0.55	0.018
677	0.18	0.005
768	0.43	0.011
764	0.57	0.018
-	0.30	0.014
-	0.87	0.016
681	0.35	0.026
687	0.40	0.011
641	0.33	0.009
670	0.38	0.010
663	0.36	0.008
619	0.39	0.010
642	0.37	0.008
623	0.40	0.010
671	0.39	0.007
631	0.38	0.008
641	0.36	0.007
614	0.38	0.008
651	0.36	0.007
590	0.32	0.008
642	0.45	0.011
689	0.44	0.011
673	0.48	0.011
671	0.36	0.017
625	0.40	0.010
662	0.33	0.008
675	0.40	0.007
622	0.34	0.007
654	0.43	0.009
777	0.41	0.008
786	0.51	0.017
763	0.27	0.008
735	0.24	0.006
745	0.33	0.010
727	0.22	0.007
784	0.54	0.014
726	0.31	0.008
760	0.34	0.010
772	0.47	0.023
743	0.50	0.011
717	0.22	0.006
782	0.36	0.010
756	0.34	0.008
780	0.44	0.011
772	0.41	0.010
699	0.17	0.006
791	0.37	0.009
779	0.54	0.014
730	0.14	0.005
770	0.43	0.009
676	0.10	0.006
793	0.42	0.012
567	0.07	0.002